

Modeling harmonic generation by a zero-range potential

W. Becker,* S. Long, and J. K. McIver

Center for Advanced Studies and Department of Physics and Astronomy, University of New Mexico, Albuquerque, New Mexico 87131

(Received 5 November 1993; revised manuscript received 28 March 1994)

High-order harmonic emission by one electron in a laser field bound to a zero-range potential is extensively discussed. The model yields an expression for the emission rates in the form of a one-dimensional integral that has to be calculated numerically. The solution is based on the quasienergy wave function of the ground state. The approach is very significantly facilitated by suppressing the harmonic components of the wave function at the position of the zero-range potential. This approximation is found to be very accurate except for the third harmonic. In spite of the simplicity of the model, the harmonic spectrum exhibits a very involved structure, occasional harmonics being strongly suppressed, with cusps and spikes for certain evenly spaced intensities. The latter are due to channel closings for the same intensities in above-threshold ionization. The harmonics near and beyond the cutoff of the plateau are amenable to a completely analytical approximation. This approximation shows how the classical model of Krause, Schafer, and Kulander [Phys. Rev. Lett. **68**, 3535 (1992)] is embedded in a fully-quantum-mechanical description. Results are also given for the harmonic production rates in an elliptically polarized laser field; they display fair agreement with recent measurements. The model should adequately describe harmonic emission by negative ions with just one bound s state. Moreover, it also gives a fair description of harmonic emission by an atom, particularly if the ground-state energy of the zero-range potential is adjusted not to the binding energy of the atom, but rather to the energy difference between the ground state and the first excited state. The reason why this is appropriate is found in lowest-order perturbation theory, which sheds some light on the physical origin of the plateau.

PACS number(s): 32.80.Rm, 42.65.Ky

I. INTRODUCTION

The behavior of atoms in intense laser fields with intensities exceeding [for neodymium-doped yttrium aluminum garnet (Nd:YAG)] 10^{13} W/cm² has revealed several unexpected and fascinating effects; for reviews see Refs. [1–9]. Among these, the production of very high harmonics of the incident laser field and, in particular, the shape of their spectrum has been possibly the most surprising discovery, largely unanticipated by any theory (for reviews see, in particular, Refs. [6] and [7]). Early experiments had already shown some emission of quite high harmonics [10–14]. However, major interest was not really generated prior to the observation that within a certain range of harmonic numbers the harmonic intensities are approximately the same and form what became epitomized as the “plateau” [15]. That is, a typical spectrum of the harmonic intensities as a function of the harmonic number exhibits a fast initial decrease followed by a region of fluctuating but on the average fairly constant intensities, viz., the plateau, with a quite well-defined upper end beyond which the intensities quickly decrease. This pattern has been, by now, established through many experiments performed at various laser frequencies and intensities on the various rare gases [16–23]. The highest

harmonics observed thus far are the 109th [21] of an 806-nm Ti-sapphire laser and the 135th [22] of a 1053-nm Nd-glass laser, both in neon.

There are several reasons why high-order harmonic generation (HHG) in atoms has attracted so much attention. First, of course, the plateau in HHG came as a surprise, posing a challenge to theory. Second, it may provide the basis for novel devices. Third, it is yet another example of the failure of lowest-order perturbation theory in high-intensity laser-atom interactions. Last but not least, the accompanying theory suggests that the plateau in the harmonic response is a very general property of driven nonlinear systems. It has emerged from calculations of model systems as different as a two-level system (which cannot be described by a potential in space), one- and three-dimensional $1/r$ potentials (having excited states and a Rydberg series), and short-range and zero-range potentials (with just one bound state). Even a one-dimensional classical harmonically driven anharmonic oscillator produces a plateau in the Fourier components of its dipole moment [7] not unlike the one observed in experiments. In spite of the generality of the phenomenon there is, to our knowledge, no equally general physical model that elucidates the physical origin of the three distinct regions of the harmonic response, viz., the initial decrease, the plateau, and the final drop off, and relates them to the parameters of the system. (This is not to say that theory has not been very successful in *reproducing* the data.) However, important progress in this regard has been made in understanding the upper end of the plateau. The number of the highest harmonic

*Present address: Physikdepartment T30, Technische Universität München, D-85747 München, Germany.

can be explained in terms of the classical nonrelativistic motion of an electron in a laser field [24,25]. It is given by $n_{\max} = (|E_0| + kU_p) / \hbar\omega$, where $|E_0|$ is the ionization energy of the atom, U_p is the ponderomotive energy of the laser field with frequency ω , and k is a number approximately equal to 3. While this result at least partially explains the physical mechanism behind the emission of the *highest* harmonics and the existence of a cutoff in the harmonic spectrum, it still leaves open the question of the origin of the plateau itself.

A complete theory of high-order harmonic generation must take into account both single-atom and collective aspects. In a microscopic description, the collective response will not exhibit any particular harmonics if the single atom does not, but high harmonics emitted by the single atom could well be suppressed in the collective response if the phases of the wave trains emitted by the individual atoms do not match. Indeed, this is the case for comparatively low intensities. Fortunately, it has turned out that for the high intensities of interest the single-atom spectrum gives a good indication of the collective response [26,27]. In this paper, we will not be concerned with the collective aspects.

There are, by now, a large number of theoretical attempts at single-atom HHG, from comparatively simple model calculations (some of which allow for almost analytical results) to hydrogen and on to realistic effective potentials for the various rare gases. However, no attempt beyond the “single-active-electron approximation” [28] has yet been made. One model that can be solved entirely analytically proceeds as follows [29]: replacing in the Hamiltonian for hydrogen in a laser field the position vector in the $\mathbf{r} \cdot \mathbf{E}$ coupling term by an appropriate multiple of the Lenz vector renders the Hamiltonian integrable. This replacement is equivalent to dropping the off-diagonal elements of \mathbf{r} . The results of this model yield a cutoff in the harmonic intensity, though not at the aforementioned proper position. Next, a two-level atom yields a spectrum whose shape shows the typical structure of high-order harmonic production [30,31]. This is particularly remarkable since the above-mentioned classical model [24,25] for the cutoff of the plateau so crucially depends on the existence of a continuum. A two-level system has also been used to model production of high harmonics from inertially confined homonuclear molecular ions [32]. A four-level system allowing for resonances has been treated as well [33]. Several one-dimensional model potentials have been investigated, most extensively the $(1+x^2)^{-1/2}$ potential [34], which preserves many features of a real atom. Numerical integration of the Schrödinger equation for this potential produced spectra in good qualitative agreement with the data [35–37]. A piecewise-constant potential allows (for electron scattering) for a largely analytical evaluation of the emitted harmonic spectrum [38]. For hydrogen and the hydrogenic ions, HHG was first attacked through lowest-order perturbation theory [39–41], which proved to be insufficient. Nonperturbative approaches followed using Floquet methods [42] or the numerical solution of the time-dependent Schrödinger equation [43,44]. For a calculation for helium that uses a model potential and pays par-

ticular attention to the effects of intermediate resonances on HHG, see Ref. [45].

State-of-the-art simulations of single-atom emission for realistic rare-gas atoms (in the context of the single-active-electron approximation) and the ensuing propagation have been pioneered and advanced by Kulander and co-workers [46–48,26,27]. These calculations start from the appropriate Hartree-Fock potential for which the time-dependent Schrödinger equation is solved on a spatial and temporal grid. Since HHG (particularly of the highest harmonics) crucially depends on minute components of the wave function, the requirements on the accuracy are very high and extreme care has to be exercised with regard to a large enough size of the grid and the choice of the boundary conditions on the boundary of the grid. Impressive examples of the deleterious effects of an insufficient grid size are given in Ref. [47]. Different forms of the dipole operator that are analytically equivalent have a large impact on the accuracy of the numerical calculation, all other things being equal [47,49]. The acceleration form has been found to be superior. Finally, after the single-atom dipole moment has been computed it is inserted in the Maxwell equations as the source of the macroscopic emission to be observed.

Two alternative approaches still ought to be mentioned. First, a purely classical treatment is able to generate a plateau as well. The dipole moment of classical Kepler orbits in the presence of the laser field when averaged over a sufficiently large ensemble produces harmonic spectra much like those that result from a quantum-mechanical treatment [50,51]. In the light of the classical model advanced to explain the upper edge of the plateau [24,25] this may not be too surprising. However, the completely classical trajectory-based description even yields satisfactory agreement for the lower harmonics. The need to average over a large number of orbits is a disadvantage of the classical method. It has been shown that in a mixed quantum-classical representation, where only the radial motion is treated classically, comparatively few trajectories suffice [52]. Finally, the Fourier transform of the dipole moment of a classical one-dimensional driven anharmonic oscillator exhibits a plateau [7] in much the same way as the quantum-mechanical two-level system.

Second, purely collective mechanisms have been suggested [53–55], which are able to generate high harmonics when the single atom does not. In the tunneling regime, most electrons are produced at those times when the electric field is at its peak, which happens at twice the laser frequency. The ionization rate as a function of time then has an almost steplike profile. Hence the electron density produced by ionization exhibits harmonics of the doubled laser frequency. The total electron current is made up by these electrons, which then quiver harmonically with the field frequency so that the total current is modulated at odd multiples of the laser frequency [53,54]. However, this mechanism does not play a major role under the conditions of the experiments carried out thus far. A very general treatment of harmonic production in a laser-irradiated plasma described by the fluid approximation has been proposed too [55].

In this paper, we will consider HHG for what may be the simplest model potential that still has some features in common with a real atom: the three-dimensional δ -function potential [56]. This potential has exactly one bound state with $l=0$ and a continuum which is, except for the s wave, unaffected by the potential. As opposed to the one-dimensional case, the δ -function potential in three dimensions requires a regularization procedure [57] in order to exhibit a well-behaved bound state. In the presence of an external plane-wave field this model potential still allows for an almost analytical solution [58–60]. Applied to HHG, emission rates can be evaluated analytically up to one final quadrature, which has to be carried out numerically. In view of the aforementioned extreme sensitivity of HHG (particularly of the highest harmonics) to the slightest numerical inaccuracies of the wave function, this is a valuable advantage. The absence of important features of a real atom, such as excited bound states and a Rydberg series, raises, of course, serious questions as to the significance of such an extremely simplified model for the analysis of HHG. However, this very deficiency can also be turned into a virtue: whatever feature is obtained from such a bare-bones atom obviously does not depend on the more subtle properties of the real atom, which were not part of the model. Moreover, at least for not too high intensities, the δ -function potential supplies a fair description of the negative hydrogen ion. In particular, it has given quite good agreement [61] with measured multiphoton detachment rates of H^- , without any adjustable parameters. Preliminary results for HHG have been published before [62,63]. In this paper, we will give a detailed account of the underlying analytical calculations, add a more extensive discussion of the results, and discuss approximations to the exact emission rates, which lend themselves to a physical interpretation. Specifically, the model atom allows for an analytical derivation of the above-mentioned “ $3U_p$ rule” for the energy of the highest harmonic. The genuine three dimensionality of the model is a decisive advantage since it allows for the description of effects that are due to the polarization of the external field. This will become particularly important for the discussion of two-color HHG to be treated in a separate paper.

The paper is organized as follows. In Sec. II, we rederive the quasienergy wave function in the presence of the external plane-wave field. This wave function is exact for a monochromatic, circularly polarized field; for any polarization other than circular, we will make some approximations which are discussed in Appendix A. In Sec. III, we employ the quasienergy wave function to derive the rates of high-order harmonic emission. The result has the form of a one-dimensional semi-infinite quadrature whose numerical evaluation requires in most cases only a few seconds computing time on a workstation. Section IV discusses the HHG rates calculated from the model as a function of its two dimensionless parameters, viz., the binding energy and the ponderomotive energy each divided by the energy of one photon. The calculated rates exhibit the general shape known from the experimental data. In particular, they have a cutoff at an energy approximately equal to $|E_0| + 3U_p$. Within the

plateau, individual harmonics may occasionally be strongly suppressed. As a function of the field intensity, the harmonic emission rates exhibit evenly spaced spikes or cusps that can be related to channel closings in the related process of above-threshold ionization. We also calculate HHG as a function of the ellipticity of the laser field and compare with recent measurements. In Sec. V, we derive an analytic approximation for the highest part of the harmonic spectrum. This approximation makes direct contact with a classical model [24,25] that attributes the highest harmonics to electrons set free in the continuum with zero velocity which subsequently are accelerated by the field and fall back into the atomic ground state upon their first recurrence to the site of the ion. The second, third, and further recurrences make up the plateau below the cutoff. However, the model fails to explain the lower portions of the plateau as well as its *a priori* existence.

Appendix A justifies an approximation that we have made for all of the explicit results: we have replaced the time dependence of the wave function at the position of the δ function, i.e., at the origin, which in principle has a Floquet expansion form with twice the frequency of the laser field, by its lowest-order term $\exp(-iEt)$. This is exact for circular polarization, but an approximation otherwise. In so much as high-order harmonic emission is concerned, this approximation turns out to have a marginal effect on all of the higher harmonics with the exception of the third. Appendix B derives a relation required in the main body of the paper. Appendix C deals with the harmonics as derived from lowest-order perturbation theory. This yields an important clue to the physical origin of the plateau: as soon as the energy of a harmonic exceeds the binding energy, multiphoton-resonant intermediate states contribute, enhancing its perturbative rate of production very significantly. Therefore, contrary to what might be considered intuitive, an increase of the harmonic emission rates with increasing harmonic order is predicted by lowest-order perturbation theory.

II. QUASIENERGY WAVE FUNCTION

In this section, for reasons of completeness, we want to rederive the quasienergy solutions for a particle bound by the zero-range potential [56,57]

$$V(\mathbf{r}) = \frac{2\pi}{\kappa m} \delta(\mathbf{r}) \frac{\partial}{\partial r} r. \quad (2.1)$$

This potential supports a single bound state with binding energy

$$E_0 = -\frac{\kappa^2}{2m} \quad (2.2)$$

and wave function

$$\psi_0(\mathbf{r}) = (\kappa/2\pi)^{1/2} \frac{e^{-\kappa r}}{r}. \quad (2.3)$$

An orthonormal set of continuum wave functions is given by

$$\psi_p(\mathbf{r}) = (2\pi)^{-3/2} \left[e^{i\mathbf{p}\cdot\mathbf{r}} - \frac{1}{\kappa + ip} \frac{e^{ipr}}{r} \right]. \quad (2.4)$$

The wave functions (2.3) and (2.4) form a complete orthonormal set.

We want to solve the time-dependent Schrödinger equation

$$i \frac{\partial}{\partial t} \Psi(\mathbf{r}t) = \left[-\frac{1}{2m} \nabla^2 + V(\mathbf{r}) - e\mathbf{r}\cdot\mathbf{E}(t) \right] \Psi(\mathbf{r}t), \quad (2.5)$$

in the presence of a time-dependent field $\mathbf{E}(t) = -\partial \mathbf{A}(t)/\partial t$. We will apply the long-wavelength approximation throughout this paper so that $\mathbf{A}(t)$ does not depend on the spatial coordinates. For the time being $\mathbf{A}(t)$ will be arbitrary, but later on we will restrict ourselves to a monochromatic field with arbitrary polarization ($-1 \leq \xi \leq 1$):

$$\mathbf{A}(t) = a(\hat{\mathbf{x}} \cos \omega t + \xi \hat{\mathbf{y}} \sin \omega t). \quad (2.6)$$

This is the long-wavelength approximation of a plane wave propagating in the z direction. We will use the length gauge in this paper. One of the reasons is that the potential (2.1), upon minimal substitution, generates a term proportional to $\delta(\mathbf{r})(-ie \mathbf{A}\cdot\mathbf{r})$, which may lead to ambiguities when applied to the wave function (2.3).

There are solutions of the Schrödinger equation (2.5) that satisfy the homogeneous integral equation

$$\Psi(\mathbf{r}t) = \int d^3\mathbf{r}' dt' G^{(E)}(\mathbf{r}t, \mathbf{r}'t') V(\mathbf{r}') \Psi(\mathbf{r}'t'), \quad (2.7)$$

where $G^{(E)}$ is the (retarded) Volkov Green's function satisfying

$$\left[i \frac{\partial}{\partial t} + \frac{1}{2m} \nabla^2 + e\mathbf{r}\cdot\mathbf{E}(t) \right] G^{(E)}(\mathbf{r}t, \mathbf{r}'t') = \delta(t-t') \delta(\mathbf{r}-\mathbf{r}'). \quad (2.8)$$

Its explicit form is

$$G^{(E)}(\mathbf{r}t, \mathbf{r}'t') = G^{(0)}(\mathbf{r}-\mathbf{r}', t-t') e^{-i\mathcal{R}(\mathbf{r}t, \mathbf{r}'t')} \times e^{-i\mathcal{M}(t, t')}, \quad (2.9)$$

where

$$G^{(0)}(\mathbf{r}, t) = \theta(t) \left[\frac{im}{2\pi(t-i\epsilon)} \right]^{3/2} \exp \left[i \frac{mr^2}{2t} \right], \quad (2.10)$$

$$\mathcal{M}(t, t') = \frac{e^2}{2m} \left[\int_{t'}^t d\tau \mathbf{A}^2(\tau) - \frac{1}{t-t'} \left[\int_{t'}^t d\tau \mathbf{A}(\tau) \right]^2 \right], \quad (2.11)$$

$$\mathcal{R}(\mathbf{r}t, \mathbf{r}'t') = e \left[\mathbf{A}(t)\cdot\mathbf{r} - \mathbf{A}(t')\cdot\mathbf{r}' - \frac{\mathbf{r}-\mathbf{r}'}{t-t'} \int_{t'}^t d\tau \mathbf{A}(\tau) \right]. \quad (2.12)$$

Equation (2.7) does not contain an inhomogeneous

term, which would allow for the specification of an initial condition as $t \rightarrow -\infty$. Instead we demand that when the field is turned off, so that $G^{(E)} \rightarrow G^{(0)}$, the solution turns into the bound-state wave function (2.3).

We now consider Eq. (2.7) specifically for the zero-range potential (2.1) for which it can be solved largely analytically [58–60]. Applying the operation $(\partial/\partial r)r$ to both sides of the integral equation (2.7) and letting $\mathbf{r}=0$, we afterwards obtain the one-dimensional integral equation

$$R(t) = \lim_{r \rightarrow 0} \frac{\partial}{\partial r} r \int_{-\infty}^t dt' G^{(E)}(\mathbf{r}t, 0t') \frac{2\pi}{\kappa m} R(t') \quad (2.13)$$

for the function

$$R(t) = \lim_{r \rightarrow 0} \frac{\partial}{\partial r} r \Psi(\mathbf{r}t). \quad (2.14)$$

The limit of $\mathbf{r} \rightarrow 0$ in Eq. (2.13) does not immediately commute with the integration since the result of the latter contains a term proportional to r^{-1} . We extract this term by writing

$$R(t) = \frac{2\pi}{\kappa m} \lim_{r \rightarrow 0} \frac{\partial}{\partial r} r \int_0^\infty d\tau \left[\frac{im}{2\pi(\tau-i\epsilon)} \right]^{3/2} \exp \left[i \frac{mr^2}{2\tau} \right] \times \{ [e^{-i\mathcal{R}(\mathbf{r}, t, 0, t-\tau)} e^{-i\mathcal{M}(t, t-\tau)} R(t-\tau) - R(t)] + R(t) \}. \quad (2.15)$$

Since

$$\int_0^\infty \frac{d\tau}{\tau^{3/2}} e^{imr^2/2\tau} = \left[\frac{2\pi i}{m} \right]^{1/2} \frac{1}{r}, \quad (2.16)$$

only the term in brackets on the right-hand side (rhs) of Eq. (2.15) contributes. This term no longer has the $\tau^{-3/2}$ singularity. The limit now commutes with the integral and we obtain

$$R(t) = -\frac{1}{\kappa} \left[\frac{m}{2\pi i} \right]^{1/2} \int_0^\infty \frac{d\tau}{\tau^{3/2}} [e^{-i\mathcal{M}(t, t-\tau)} R(t-\tau) - R(t)]. \quad (2.17)$$

For the monochromatic circularly polarized field (2.6) (with $\xi=1$) the function

$$\mathcal{M}(t, t-\tau) = \frac{(ea)^2}{2m} \tau \left[1 - \left[\frac{\sin(\omega\tau/2)}{\omega\tau/2} \right]^2 \right] \equiv \mathcal{M}(\tau) \quad (2.18)$$

depends only on the difference of its arguments, viz., on τ . In this case, Eq. (2.17) is solved by the exponential

$$R(t) \sim e^{-iEt}, \quad (2.19)$$

where the quasienergy E is to be determined from the integral equation

$$\kappa = - \left[\frac{m}{2\pi i} \right]^{1/2} \int_0^\infty \frac{d\tau}{\tau^{3/2}} (e^{iE\tau} e^{-i\mathcal{M}(\tau)} - 1). \quad (2.20)$$

If the field is turned off we have $\mathcal{M}(\tau) \equiv 0$, and Eq. (2.20) yields, as it should,

$$E = E_0 = -\frac{\kappa^2}{2m} . \tag{2.21}$$

In the presence of the field the quasienergy is complex,

$$E = -|E_0| + \Delta E - i\Gamma/2 . \tag{2.22}$$

The quantity ΔE is the Stark shift of the ground state and the imaginary part Γ specifies the ionization rate. It must be positive in order that, in view of Eq. (2.19), the ground state be depleted by ionization. However, if

$\Gamma > 0$, the integral on the rhs of Eq. (2.20) diverges. This characteristic difficulty has been noticed long ago. A solution (2.22) of Eq. (2.20) must be sought through analytic continuation. The details as well as practical methods of how to determine the quasienergy are discussed elsewhere [64].

For any polarization other than circular the function $\mathcal{M}(t, t - \tau)$ depends on both arguments separately and a simple exponential no longer solves Eq. (2.17). For the vector potential (2.6) we have, for arbitrary ξ ,

$$\mathcal{M}(t, t') = \eta \left\{ \omega(t-t') \left[1 - \left[\frac{\sin(\omega(t-t')/2)}{\omega(t-t')/2} \right]^2 \right] + \xi \cos\omega(t+t') \left[\sin\omega(t-t') - \frac{4 \sin^2(\omega(t-t')/2)}{\omega(t-t')} \right] \right\} , \tag{2.23}$$

where we introduced the ponderomotive potential

$$U_p = \frac{e^2 \langle \mathbf{A}^2 \rangle}{2m} = \frac{(ea)^2}{4m} (1 + \xi^2) \equiv \omega\eta \tag{2.24}$$

and the parameter

$$\xi = \frac{1 - \xi^2}{1 + \xi^2} . \tag{2.25}$$

In place of the ansatz (2.19) we now have to allow for a Floquet expansion,

$$R(t) = e^{-iEt} \sum_{n=-\infty}^{\infty} a_n e^{2in\omega t} \equiv e^{-iEt} w(t) . \tag{2.26}$$

Inserting this into Eq. (2.17) and expanding the exponential of the second term on the rhs of Eq. (2.23) in terms of Bessel functions, we get

$$\kappa a_n = - \left[\frac{m}{2\pi i} \right]^{1/2} \sum_{k=-\infty}^{\infty} a_k \int_0^{\infty} \frac{d\tau}{\tau^{3/2}} (e^{i[E' - (k+n)\omega]\tau} e^{4i\eta \sin^2(\omega\tau/2)/(\tau\omega)} i^{n-k} J_{k-n}(z(\tau)) - \delta_{kn}) , \tag{2.27}$$

where

$$z(\tau) = \eta\xi \left[\sin\omega\tau - \frac{4 \sin^2(\omega\tau/2)}{\omega\tau} \right] \tag{2.28}$$

and

$$E' = E - U_p . \tag{2.29}$$

Subtracting and adding $\delta_{kn} \exp(i(E' - 2n\omega)\tau)$ under the integral in Eq. (2.27) yields

$$[(-E' + 2n\omega)^{1/2} - |E_0|^{1/2}] a_n = \sum_{k=-\infty}^{\infty} R_{nk} a_k , \tag{2.30}$$

with

$$R_{nk} = (4\pi i)^{-1/2} \int_0^{\infty} \frac{d\tau}{\tau^{3/2}} e^{i[E' - (k+n)\omega]\tau} [e^{4i\eta \sin^2(\omega\tau/2)/(\tau\omega)} i^{n-k} J_{k-n}(z(\tau)) - \delta_{kn}] . \tag{2.31}$$

We notice the symmetry properties

$$R_{nk} = R_{kn} \tag{2.32}$$

and

$$R_{n+l, k+l}(E') = R_{nk}(E' - 2l\omega) . \tag{2.33}$$

The quasienergy is determined from the condition that the determinant of the infinite linear system (2.30) be zero, viz.,

$$\det \{ [(-E' + 2n\omega)^{1/2} - |E_0|^{1/2}] \delta_{nm} - R_{nm} \} = 0 . \tag{2.34}$$

As a consequence of the symmetry property (2.33), whenever E' is a solution of Eq. (2.34) then so too is $E' + 2n\omega$ with integer n . We define as the quasienergy the particular solution of Eq. (2.34) that reduces to $-|E_0|$ for vanishing field.

In perturbation theory with respect to the intensity, viz., η , the integrals (2.31) go as

$$R_{nk} \sim \begin{cases} \eta^{|n-k|}, & n \neq k \\ \eta, & n = k \end{cases} \quad (2.35)$$

The lowest approximation to the solution of the determinant equation (2.34) then consists in just keeping the diagonal. In this case, the quasienergy as defined above is given by the solution of

$$(-E')^{1/2} - |E_0|^{1/2} = R_{00}(E'). \quad (2.36)$$

The corresponding approximation for the expansion coefficients is $a_0 \neq 0$, $a_n = 0$ for $n \neq 0$. In a next step, we may keep terms in Eq. (2.34) with $|n-m|=1$ so that the resulting matrix has tridiagonal form. The quasienergy is then determined by

$$\sum_n \frac{R_{n,n+1}^2}{(-E' + 2n\omega)^{1/2} - |E_0|^{1/2} - R_{nn}} \times \frac{1}{[-E' + 2(n+1)\omega]^{1/2} - |E_0|^{1/2} - R_{n+1,n+1}} = 1. \quad (2.37)$$

Here, it is a good approximation just to keep the terms with $n=0$ and $n=-1$. This yields the equation

$$\begin{aligned} & (-E')^{1/2} - |E_0|^{1/2} - R_{00} \\ &= \frac{R_{01}^2}{(-E' + 2\omega)^{1/2} - |E_0|^{1/2} - R_{11}} \\ &+ \frac{R_{-1,0}^2}{(-E' + 2\omega)^{1/2} - |E_0|^{1/2} - R_{-1,-1}}, \end{aligned} \quad (2.38)$$

which improves on Eq. (2.36). The expansion coefficients a_1 and a_{-1} can then be determined from a_0 through Eq. (2.30). All other a_n are still zero in this approximation.

The quasienergy wave function of the ground state is given by Eqs. (2.7), (2.14), and (2.26):

$$\Psi(\mathbf{r}t) = \frac{2\pi}{\kappa m} \int_{-\infty}^t dt' G^{(E)}(\mathbf{r}t, 0, t') e^{-iEt'} w(t'). \quad (2.39)$$

For most applications, we will replace the quasienergy E on the right-hand side of Eq. (2.39) which, in principle, has to be determined from Eq. (2.34) by its field-free value of $-|E_0|$. We thereby neglect the small ac Stark shift of the ground state. The ponderomotive shift of the continuum states is unaffected by this approximation, since it is contained in the propagator $G^{(E)}$. We will also let $a_n = 0$ for $n \neq 0$ and determine a_0 from the normalization of the ground-state wave function (2.3) in the absence of the field, so that

$$a_0 = \kappa(\kappa/2\pi)^{1/2} = (2\pi)^{-1/2} (2m|E_0|)^{3/4}. \quad (2.40)$$

III. EMISSION OF HARMONICS

Having determined the wave function (2.39) of the ground state dressed by the external field (2.6) we are in a position to calculate the rates for emission of harmonics. Initially, the "atom" is in its dressed ground state with wave function (2.39). At time t it emits a photon with

frequency Ω and polarization ϵ and thereby ends up in some final state $\Psi_f(\mathbf{r}t)$ dressed again by the field. The S matrix element governing this process is

$$M = -i \left[\frac{2\pi\Omega}{V} \right]^{1/2} \int d^3r dt e^{i\Omega t} [\Psi_f(\mathbf{r}t)]^* \times (-e\mathbf{r} \cdot \epsilon)^* \Psi(\mathbf{r}t), \quad (3.1)$$

where V is some normalization volume. Several remarks are in order here. (i) The final state can, in principle, be any excited state of the atom as well as the ground state, each dressed by the field. It can be a continuum state as well [65]. For any final state other than the ground state we consider the combined process of excitation or ionization plus harmonic production. However, unless the excited state is resonant with a multiple of the laser frequency, the emitted frequencies Ω would not be harmonics of the laser frequency ω . While certainly possible, to our knowledge such emission has never been observed. Excited bound states do not exist for our model atom, anyway. For these reasons, we will only consider emission processes where the atom, after the emission, returns to its dressed ground state so that $\Psi_f \equiv \Psi$. If $\Psi(\mathbf{r}t)$ were an eigenstate of energy the matrix element (3.1) would be zero. But since the state $\Psi(\mathbf{r}t)$ is dressed by the field it is not an eigenstate of energy. The matrix element is then proportional to the Fourier transform of the dipole moment of the ground state:

$$M = i \left[\frac{2\pi\Omega}{V} \right]^{1/2} \epsilon^* \cdot \mathbf{d}(\Omega), \quad (3.2)$$

$$\begin{aligned} \mathbf{d}(\Omega) &= \int dt e^{i\Omega t} \mathbf{d}(t) \\ &= \int dt d^3r e^{i\Omega t} [\Psi(\mathbf{r}t)]^* e\mathbf{r} \Psi(\mathbf{r}t). \end{aligned} \quad (3.3)$$

Most often, the dipole moment $\mathbf{d}(\Omega)$ is used as the starting point of the calculation of harmonic emission since it acts as the source term for HHG in Maxwell's equations. We have here preferred to start from the S -matrix element (3.1) because it would allow for final states other than the ground state as well.

(ii) We use the long-wavelength approximation for the emitted field as well as for the laser field, thereby suppressing higher-order multipole emission. It would not be too difficult to use $\exp[i(\Omega t - \mathbf{K} \cdot \mathbf{r})]$ in place of $\exp(i\Omega t)$ in Eq. (3.1). However, consistency might then demand us to treat the laser field without the dipole approximation too. This, in turn, may require a relativistic description in order to avoid artifacts that can occur if one uses a field transforming under the Lorentz group in the context of the nonrelativistic Schrödinger equation. (iii) It is not difficult to convince oneself that the matrix element M can also be expressed in terms of the $\mathbf{p} \cdot \mathbf{A}$ interaction for the emitted photon:

$$M = \left[\frac{2\pi}{\Omega V} \right]^{1/2} \int d^3r dt e^{i\Omega t} [\Psi(\mathbf{r}t)]^* \left[-\frac{e}{m} \epsilon \cdot \mathbf{p} \right]^* \times \Psi(\mathbf{r}t). \quad (3.4)$$

(iv) The matrix element (3.1) or (3.4) is related to the ex-

pectation value of the dipole moment rather than the dipole-dipole correlation function. It has been argued that the latter should be used in place of the former. This would be true if we were interested in HHG of just one single atom. However, by using the quasienergy wave function (2.39) we already tacitly assume that we are interested in an appropriate ensemble of uncorrelated atoms averaged over initial conditions. It has been shown that in this case the expectation value of the dipole moment is the relevant quantity [30,66].

In view of Eq. (2.39) the Fourier transform (3.3) of the dipole moment can be written in the form

$$\mathbf{d}(\Omega) = -\frac{ie}{m} \left[\frac{2\pi}{\kappa m} \right]^2 \left[\frac{im}{2\pi} \right]^{3/2} \int_{-\infty}^{\infty} dt e^{i\Omega t} \int_{-\infty}^t dt' dt'' (t' - t'' - i\epsilon)^{-5/2} \times e^{-i(Et'' - E^*t')} [w(t')]^* w(t'') \mathcal{F}(t; t', t'') e^{-i\mathcal{M}(t', t'')}, \quad (3.7)$$

with

$$\mathcal{F}(t; t', t'') = e^{i(t-t'')} \int_{t'}^t d\tau \mathbf{A}(\tau) + e^{i(t'-t)} \int_{t''}^{t'} d\tau \mathbf{A}(\tau). \quad (3.8)$$

This still holds for an arbitrary vector potential $\mathbf{A}(t)$. A similar model that produces a dipole moment closely related to Eq. (3.7) has recently been proposed [76].

In order to make further progress we have to specify the vector potential. For the monochromatic field (2.6) with arbitrary elliptic polarization the function $\mathcal{M}(t, t')$ has already been given in Eq. (2.23). It is convenient to introduce the variables

$$\tau' = t - t', \quad \tau'' = t - t'' \quad (0 \leq \tau', \tau'' < \infty), \quad (3.9) \quad \text{and}$$

$$\mathcal{F}(t; t', t'') = \frac{ea}{2i\omega^2} \left\{ e^{i\omega t(\hat{\mathbf{x}} - i\xi\hat{\mathbf{y}})} \left[-\tau + e^{-i\sigma/2} \left[\tau \cos \frac{\tau}{2} + i\sigma \sin \frac{\tau}{2} \right] \right] - \text{c.c.} \right\}. \quad (3.12)$$

We can now do the integration over t in Eq. (3.7). For simplicity, we will neglect the width Γ and Stark shift ΔE of the ground states discussed in Sec. II (see, however, the remark below regarding emission, viz., scattering of the fundamental). After some algebra, the dipole moment can be written as

$$\begin{aligned} \mathbf{d}(\Omega) = & -2\pi i \frac{e^2 a}{4m} \left[\frac{2\pi}{\kappa m} \right]^2 \left[\frac{im}{2\pi\omega} \right]^{3/2} \sum_{k,n,l} \delta(\Omega - 2\omega(k+n) - \omega) a_{n+l}^* a_l i^k \\ & \times \int_{-\infty}^{\infty} \frac{d\tau}{(\tau + i\epsilon)^{5/2}} \int_{|\tau|}^{\infty} d\sigma e^{i(n+k)\sigma} e^{i(|E_0|/\omega + n+2l)\tau} \exp \left\{ i\eta\tau \left[1 - \left[\frac{\sin(\tau/2)}{\tau/2} \right]^2 \right] \right\} \\ & \times \left\{ i(\hat{\mathbf{x}} - i\xi\hat{\mathbf{y}}) J_{k+1}(z(\tau)) \left[-\tau e^{i\sigma} + e^{i\sigma/2} \left[\tau \cos \frac{\tau}{2} + i\sigma \sin \frac{\tau}{2} \right] \right] \right. \\ & \left. - (\hat{\mathbf{x}} + i\xi\hat{\mathbf{y}}) J_k(z(\tau)) \left[-\tau + e^{i\sigma/2} \left[\tau \cos \frac{\tau}{2} - i\sigma \sin \frac{\tau}{2} \right] \right] \right\}, \quad (3.13) \end{aligned}$$

where $z(\tau)$ is given by Eq. (2.28) with $\omega\tau$ replaced by τ as defined in Eq. (3.10). The a_n are the Fourier expansion coefficients of the function $w(t)$ defined in Eq. (2.26). Finally, we can carry out the integration over σ , which leaves

$$\begin{aligned} \mathbf{d}(\Omega) = & \left[\frac{2\pi}{\kappa m} \right]^2 \int dt e^{i\Omega t} \int_{-\infty}^t dt' dt'' e^{-i(Et'' - E^*t')} \\ & \times [w(t')]^* w(t'') \\ & \times \mathbf{d}(t; t', t''). \quad (3.5) \end{aligned}$$

The spatial integral

$$\mathbf{d}(t; t', t'') = \int d^3r [G^{(E)}(\mathbf{r}t; 0, t')]^* e \mathbf{r} G^{(E)}(\mathbf{r}t; 0, t'') \quad (3.6)$$

can be reexpressed in terms of $G^{(E)}$ as shown in Appendix B. With the help of Eqs. (B5) and (B4) we arrive at

and the dimensionless sum and difference variables

$$\begin{aligned} \tau &= \omega(\tau' - \tau'') \quad (-\infty < \tau < \infty), \\ \sigma &= \omega(\tau' + \tau'') \quad (|\tau| \leq \sigma < \infty). \end{aligned} \quad (3.10)$$

In terms of these and the parameters introduced above in Eqs. (2.24) and (2.25), we have

$$\begin{aligned} \mathcal{M}(t', t'') = & -\eta \left\{ \tau \left[1 - \left[\frac{\sin \tau/2}{\tau/2} \right]^2 \right] \right. \\ & \left. + \zeta \cos(2\omega t - \sigma) \left[\sin \tau - \frac{4}{\tau} \sin^2 \frac{\tau}{2} \right] \right\} \quad (3.11) \end{aligned}$$

$$\begin{aligned}
\mathbf{d}(\Omega) = & 2\pi \frac{e^2 a}{4m} \left[\frac{2\pi}{m\kappa} \right]^2 \left[\frac{im}{2\pi\omega} \right]^{3/2} \left[\frac{2\omega}{\Omega} \right]^2 \sum_{k,n,l} a_{n+l}^* a_l i^k \delta(\Omega - (2k+1)\omega) \\
& \times \int_{-\infty}^{\infty} \frac{d\tau}{(\tau+i\epsilon)^{5/2}} e^{i(|E_0|/\omega+n+2l)\tau} e^{i\eta\tau\{1-[\sin(\tau/2)/(\tau/2)]^2\}} e^{i\Omega|\tau|/(2\omega)} \\
& \times \left\{ i(\hat{\mathbf{x}} - i\xi\hat{\mathbf{y}}) J_{k-n+1}(z(\tau)) \left[\frac{\tau e^{i|\tau|/2}}{2(1+\omega/\Omega)} - \sin \frac{\tau}{2} \right] \right. \\
& \left. + (\hat{\mathbf{x}} + i\xi\hat{\mathbf{y}}) J_{k-n}(z(\tau)) \left[\frac{\tau e^{-i|\tau|/2}}{2(1-\omega/\Omega)} - \sin \frac{\tau}{2} \right] \right\}. \tag{3.14}
\end{aligned}$$

Through Eq. (3.2) the dipole moment $\mathbf{d}(\Omega)$ is proportional to the matrix element for emission of a photon with frequency Ω and polarization ϵ . It displays a sequence of odd harmonics of the laser frequency ω , whose strength has to be determined by the one remaining quadrature with respect to τ . For an elliptically polarized incident field ($0 < |\xi| < 1$) the polarization of the emitted harmonics is elliptical too. For linear polarization ($\xi=0$) it is linear. For circular polarization ($|\xi|=1$) we have $z(\tau)=0$. As a consequence, $a_n=0$ for $n \neq 0$ and no harmonics are emitted. Equation (3.14) does not allow for the calculation of the scattering of the fundamental, owing to the divergence of the last square bracket for $\Omega=\omega$. This can be traced back to our neglecting the width Γ . In order to compute scattering of the fundamental, this width, but also, and more importantly, other existing damping mechanisms, would have to be included.

It is more convenient to restrict the remaining integration in Eq. (3.14) to positive values of τ . Such a form is

$$\begin{aligned}
\mathbf{d}(\Omega) = & \frac{2e^2 a}{\kappa^2} \left[\frac{2\pi}{m\omega} \right]^{3/2} \left[\frac{\omega}{\Omega} \right]^2 \sum_k \delta(\Omega - (2k+1)\omega) \\
& \times \sum_{nl} a_{n+l}^* a_l i^{2k+n} \int_0^{\infty} \frac{d\tau}{\tau^{3/2}} e^{i\Omega\tau/(2\omega)} \\
& \times \{ (\hat{\mathbf{x}} - i\xi\hat{\mathbf{y}}) J_{k-n+1}(z(\tau)) \beta_+(\tau) \sin(\alpha_{knl}(\tau)) \\
& - (\hat{\mathbf{x}} + i\xi\hat{\mathbf{y}}) J_{k-n}(z(\tau)) \beta_-(\tau) \cos(\alpha_{knl}(\tau)) \} \\
= & \sum_k \mathbf{d}_k \delta(\Omega - (2k+1)\omega), \tag{3.15}
\end{aligned}$$

where

$$\beta_{\pm}(\tau) = \frac{e^{\pm i\tau/2}}{1 \pm \omega/\Omega} - \frac{2}{\tau} \sin \frac{\tau}{2}, \tag{3.16}$$

$$\begin{aligned}
\alpha_{knl}(\tau) = & \left[\frac{|E_0|}{\omega} + n + 2l \right] \tau + \eta\tau \left[1 - \left[\frac{\sin \tau/2}{\tau/2} \right]^2 \right] \\
& - \frac{\pi}{4} - \frac{\pi}{2}(n+k), \tag{3.17}
\end{aligned}$$

and $z(\tau)$ is defined in Eq. (2.28) (with $\omega\tau \rightarrow \tau$). In Eq. (3.15) the terms with $n=k+1$ and $n=k$ apparently give rise to a divergence at $\tau=0$ since $J_0(0)=1$. If these terms are to be kept, one has to go back to Eq. (3.14). There is no actual divergence since $\int_{-\infty}^{\infty} d\tau (\tau+i\epsilon)^{-3/2} = 0$.

Finally, we square the matrix element (3.1), multiply with the phase-space density of the emitted photon with momentum \mathbf{K} ($|\mathbf{K}|=\Omega$), divide by a long normalization time, and integrate over the energy-conserving δ function of the $(2k+1)$ st harmonic. This yields the rate of emis-

sion per unit time and solid angle of a photon of the $(2k+1)$ st harmonic with polarization ϵ ,

$$\frac{dR_{2k+1}}{d\Omega_{\mathbf{K}}} = \left[\frac{(2k+1)\omega}{2\pi} \right]^3 |\epsilon^* \cdot \mathbf{d}_k|^2. \tag{3.18}$$

IV. PROPERTIES OF THE EMITTED HARMONICS

In this section we will present and discuss the spectral intensities of the emitted higher harmonics as a function of the two dimensionless parameters of the model $\epsilon = |E_0|/\hbar\omega$ and $\eta = U_p/\hbar\omega$. To this end the one remaining quadrature in the expression for the induced dipole moment has to be carried out numerically. For all the results presented in what follows we will start from Eq. (3.15) with the approximation discussed in Appendix A that $a_n = \delta_{n0} a_0$, where a_0 is given by Eq. (2.40). Most of the time we will deal with purely linear polarization $\xi=1$. In this case, the dipole moment (3.15) reduces to

$$\begin{aligned}
\mathbf{d}(\Omega) = & \frac{8e}{\omega} (\pi\eta|E_0|/m)^{1/2} \sum_k \frac{(-1)^k}{(2k+1)^2} \delta(\Omega - (2k+1)\omega) \int_0^{\infty} \frac{d\tau}{\tau^{3/2}} e^{i(k+1/2)\tau} \\
& \times [J_{k+1}(z(\tau)) \beta_+(\tau) \sin \alpha_{k00}(\tau) - J_k(z(\tau)) \beta_-(\tau) \cos \alpha_{k00}(\tau)]. \tag{4.1}
\end{aligned}$$

In order to make contact with the notation used previously [62,63], we note that

$$d(\Omega) = 2e \left(\frac{\pi}{m\omega} \right)^{1/2} \hat{\mathbf{x}} \sum_k \delta(\Omega - (2k+1)\omega) L_k^* \quad (4.2)$$

The differential emission rate per unit time and solid angle (3.18) then reduces to

$$\frac{dR_{2k+1}}{d\Omega_{\mathbf{k}}} = \omega \frac{r_0}{\pi\lambda} (2k+1)^3 \epsilon_x^2 |L_k|^2 \quad (4.3)$$

Here the dimension is carried by the factor of ω , $r_0 = e^2/m$ is the classical electron radius, and $\lambda = 2\pi/\omega$ is the laser wavelength. The fact that the dimensionless quantity $|L_k|^2$ only depends on the two dimensionless parameters ϵ and η implies scaling laws for the emission rate (4.3).

The dipole moment (4.1) vanishes with vanishing $|E_0|$, as it should; in the nonrelativistic domain under investigation here, an electron that is just subject to the field and not to any third agent moves harmonically and does not radiate any higher harmonics. However, the dipole moment goes to zero only as the square root of $|E_0|$. Hence, we will see below, even for very small binding energies there is still substantial harmonic emission. Owing to rapid depletion of the ground state, however, which we neglected by the approximation $\Gamma=0$, these results are only physically meaningful in the limit where the pulse length goes to zero.

Figures 1 and 2 display typical results. Figure 1 shows the harmonics emitted by a model atom with the binding energy of argon ($|E_0|=15.76$ eV) in a Nd:YAG laser ($\hbar\omega=1.165$ eV) for several intensities and Fig. 2 compares various model atoms with different binding energies while the intensity is fixed. All of the spectra show the end of the plateau at a harmonic number near $(|E_0|+3U_p)/\hbar\omega$. Figure 2 indicates that the height of the plateau, that is, the efficiency of HHG, drops dramatically with increasing ϵ . Therefore, e.g., doubling ω for constant $|E_0|$ boosts the efficiency of HHG even if η ,

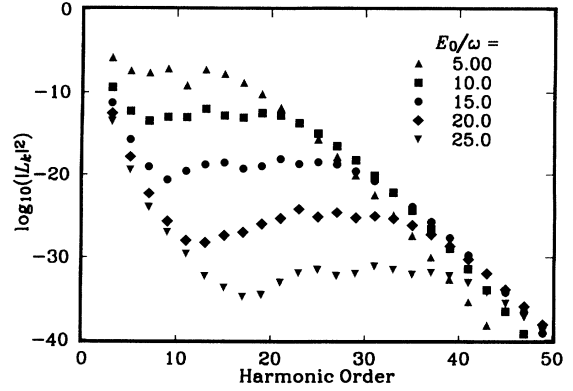


FIG. 2. $\log_{10}(|L_k|^2)$ as a function of harmonic order $(2k+1)$ for an intensity of 3×10^{13} W/cm² in YAG ($\eta=2.7$) with $|E_0|=5, 10, 15, 20,$ and $25\hbar\omega$.

which scales as ω^{-3} , decreases in the process. Figures 2 and 6 show that the height of the plateau scales less dramatically with η , particularly for $\eta \gg 1$. Unfortunately, however, the extent of the plateau thereby reduces significantly since its maximal energy is approximately $|E_0|+3U_p$.

As a general feature, the intensities within the plateau region fluctuate by up to one order of magnitude from one harmonic to the next and in some cases even more. For example, Fig. 1 shows that the 15th harmonic in “argon” is suppressed by about two orders of magnitude with respect to the two neighboring harmonics. This effect is pursued more closely in Fig. 3 with the result that this suppression takes place in the intensity region $2 \leq \eta \leq 5$. It is amusing to observe that experimentally the 13th harmonic in argon in the situation covered by Fig. 1 has not been detected in the earlier measurements [16] and has just barely been seen recently [67], about one order of magnitude below the average level of the plateau. The near agreement with the data may well be accidental. However, the fact that these features occur for the bare-bones δ -function atom proves that they are not

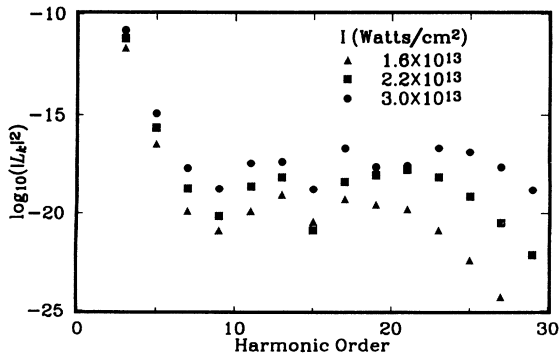


FIG. 1. $\log_{10}(|L_k|^2)$ as a function of the harmonic order $(2k+1)$ for argon ($|E_0|=15.76$ eV) in YAG ($\hbar\omega=1.165$ eV) for three different intensities. The rate of emission is proportional to $(2k+1)^3 |L_k|^2$.

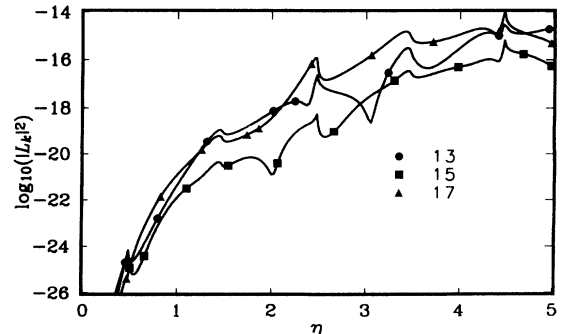


FIG. 3. $\log_{10}(|L_k|^2)$ as a function of intensity for the 13th, 15th, and 17th harmonics for argon ($|E_0|=15.76$ eV) in YAG. Throughout most of the intensity range, the 15th harmonic is significantly suppressed with respect to its neighbors.

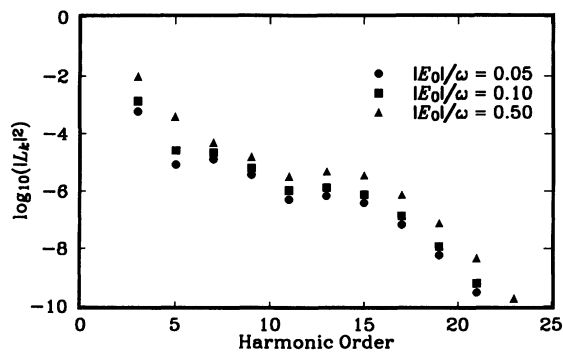


FIG. 4. $\log_{10}(|L_k|^2)$ as a function of harmonic order $(2k+1)$ for $\eta=5$ and with binding energies $|E_0|=0.05, 0.1$, and $0.5\hbar\omega$.

necessarily related to resonances, Rydberg series, or other more subtle properties of real atoms and/or fields. Just one bound state, a continuum, and a plane-wave field of infinite extent are sufficient to generate them.

Figure 4 shows the harmonic spectra for extremely low binding energies. The plateau still obeys the “ $3U_p$ rule.” The figure also vividly illustrates the fact that even though no harmonics are emitted for $|E_0|=0$, they die out only very slowly when $|E_0|$ approaches zero. Of course, these results are rather academic as atoms with binding energies this low can only be exposed for the intensities under consideration to extremely short pulses before they ionize.

In contrast to their rugged structure within the plateau, the harmonics drop very smoothly beyond its end. In Fig. 5, we have plotted the number of the “last” harmonic, defined as the last local maximum of the harmonic intensities versus η . The straight line $n_{\max}=(|E_0|+3.17U_p)/\hbar\omega$ provides an almost perfect fit up to very high intensities. We will investigate this rule more closely in Sec. V and relate it to the properties of the integral (3.15) and a simple physical model [24,25]. The $3U_p$ rule agrees quite well with the data [22,24]; significant deviations have been attributed to harmonic emission from the respective ions [24].

While the δ potential when applied to real atoms can at

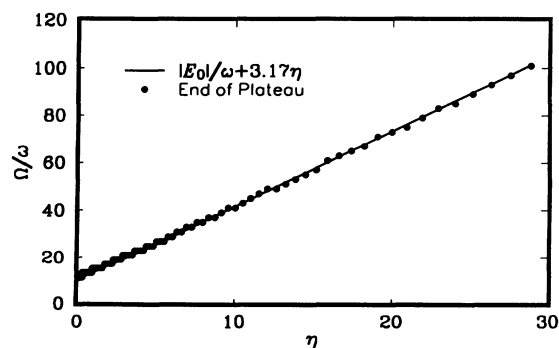


FIG. 5. End of the plateau, defined as the last local maximum of the harmonic emission rates, as a function of the intensity for $|E_0|/\hbar\omega=10$. The straight line $\Omega=|E_0|+3.17U_p$ provides a perfect fit.

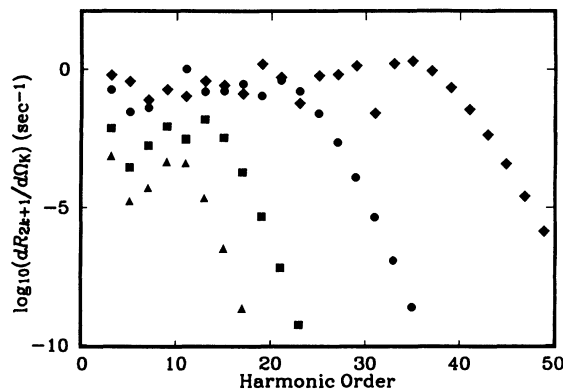


FIG. 6. Single-atom harmonic emission rate for H^- in a CO_2 laser at intensities 1, 2, 5, and $10 \times 10^{10} \text{ W/cm}^2$.

best be expected to pinpoint some trends and some general features, it constitutes a reasonable model of the negative hydrogen ion to the extent that the former can be described as an effective one-electron system. This should be possible for not too high intensities. Indeed, multiphoton detachment of H^- has been successfully modeled with the δ -function potential [61]. However, for intensities approaching the stabilization regime the description by an effective one-electron potential is known to break down [68,69]. No experiments on higher harmonic generation in H^- have been carried out yet. In Fig. 6 we show the harmonic production rates for H^- ($|E_0|=0.754 \text{ eV}$) in a CO_2 laser for various intensities. Of course, experimental results for H^- would be highly interesting since they would for the first time deal with harmonic production from a non-Coulombic (short-range) potential.

The dependence of a given harmonic on the intensity displays the same rugged nature as the plateau for a given intensity. In Fig. 7 the 19th harmonics for “krypton” and “argon” in Nd:YAG ($\epsilon=12.01$ and 13.52 , respectively) are plotted versus η . Two distinct patterns are immediately distinguished. First, there are pronounced spikes spaced by integer intervals in η . Second, the emis-

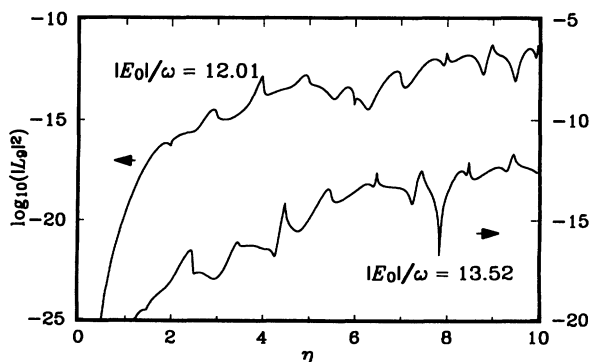


FIG. 7. $\log_{10}(|L_9|^2)$ as a function of laser intensity for $|E_0|/\hbar\omega=12.01$ (krypton) and $|E_0|/\hbar\omega=13.52$ (argon). The evenly (in η) spaced spikes or cusps which are visible for $\eta=(\text{integer})-0.01$ for krypton and $\eta=(\text{integer})-0.52$ for argon are related to the closings of ATI channels.

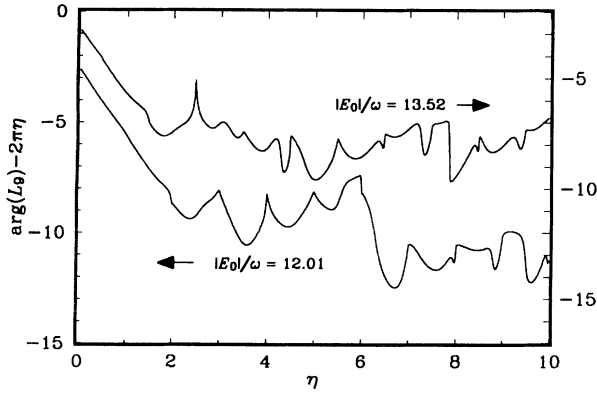


FIG. 8. Phase of L_9 as a function of intensity for the same situation as in Fig. 7. Since the phase changes on the average by 2π when η increases by 1 in the plateau region, the quantity $\arg(L_9) - 2\pi\eta$ is plotted.

sion rate drops occasionally by several orders of magnitude, e.g., for krypton at $\eta \approx 6.5$ and $\eta \approx 9.5$ and for argon at $\eta \approx 4.8$ and $\eta \approx 7.9$. Figure 8 gives the phase of L_9 for the same situation. We can infer a close correspondence between these patterns in the magnitude and in the phase of L_9 . The physical origin of the integer-spaced spikes has been explained in Ref. [63]. They occur at those intensities where an above threshold ionization (ATI) channel corresponding to the absorption of a specific number of photons closes owing to the ponderomotive barrier increasing with intensity. These channel closings occur at

$$|E_0| + U_p = n\hbar\omega$$

or

$$\epsilon + \eta = n, \quad (4.4)$$

i.e., in the case of Fig. 7 at $\eta = n - 0.01$ for $\epsilon = 12.01$ and at $\eta = n - 0.52$ for $\epsilon = 13.52$. In the phase of L_k these channel closings show up as a sudden temporary decrease of the phase. The spikes only occur for the harmonics within the plateau and not for those beyond. For Fig. 7, the 19th harmonic for $\epsilon = 12.01$ is outside the plateau for $\eta \sim 2.5$, and we can see how in this region the spikes disappear and the slope of the phase settles to a value near 3.3 (to be explained in Sec. V). It is interesting to notice that approximately integer-spaced structures (spikes or resonances) have also emerged from single-atom calculations based on a numerical solution of the time-dependent Schrödinger equation (see Ref. [27] for xenon and Ref. [47] for hydrogen) and to some extent have also been seen experimentally [67]. Attributing experimentally observed structures in the intensity dependence to patterns calculated for single atoms at constant intensity cannot really be done without properly averaging over the intensity distribution in the interaction region.

In view of the above, we expect that the harmonic emission rates are much smoother when $\eta + \epsilon$ is kept constant while either η or ϵ is varied. This expected behavior is displayed in Fig. 9, where $\eta + \epsilon = 13.57$ and η

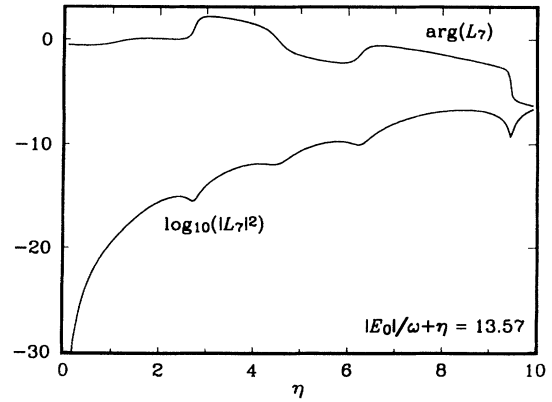


FIG. 9. Argument and phase of L_7 as a function of η when $\epsilon + \eta = 13.57$ is kept constant. The spikes related to the channel closings are absent.

is varied. Indeed, the spikes related to channel closings are now absent. We have no explanation for the quite pronounced structures that still remain and the associated suppressions of the harmonic emission rates.

Figures 10, 11, and 12 deal with the effects of the polarization of the incident laser field (2.6) on the spectrum of the emitted harmonics. Figure 10 shows the decrease of the harmonic response with increasing ellipticity of the laser field. Both the intensities of the electric field of the harmonics in the x direction and in the y direction are given. We notice that both components have the same cutoff, which is approximately given by Eq. (5.24), viz.,

$$E_{\max} = |E_0| + 3.17U_p / (1 + \xi^2). \quad (4.5)$$

The fact that the components of the harmonic intensities in the two directions have the same cutoff implies that

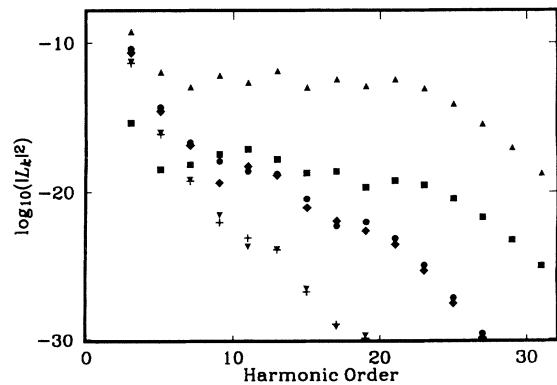


FIG. 10. Harmonic emission rates for the case where the polarization of the driving laser field [given by Eq. (2.6)] changes from linear to circular for $|E_0|/\omega = 10$ and $\eta = 3$. The topmost triangles and the squares correspond to $\xi = 0.001$ for polarization along the x and y axes, respectively. (The topmost triangles agree up to three digits with the case where $\xi = 0$, viz., linear polarization.) The circles and diamonds are for $\xi = 0.5$, for x and y polarization, respectively, and the plusses and lower triangles for $\xi = 0.9$.

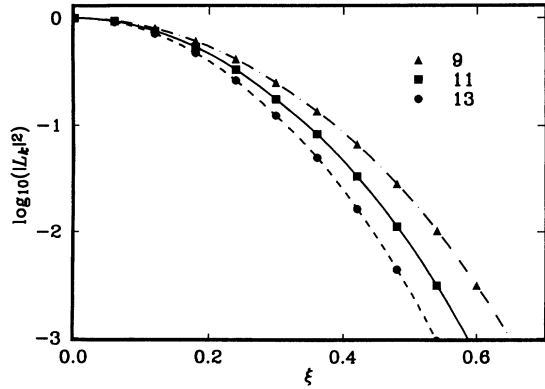


FIG. 11. Harmonic emission rate of various harmonics vs ellipticity ξ , for $|E_0|/\omega=4$, $\eta=1$. The figure corresponds to Fig. 1 of Ref. [74] (xenon, 600 nm).

throughout the harmonic spectrum the polarization of the emitted harmonics is roughly similar to the incident laser field. For example, for $\xi=0.001$, i.e., when the laser field is practically linearly polarized, the y intensity is lower than the x intensity on the average by a factor of $10^6=\xi^{-2}$. Figures 11 and 12 correspond to recent measurements and will be discussed below.

How well does this model fare when in spite of the above-mentioned reservations a quantitative comparison with the data is attempted? We can get a partial answer from a numerical comparison between the hydrogenic Coulomb potential and a Yukawa potential whose parameters are adjusted such that it supports exactly one bound state with a binding energy equal to the ground state of hydrogen. Figure 6 of Ref. [47] (see also Fig. 13 of this paper) shows that for a fixed intensity of 2×10^{13} W/cm² and 1064 nm the Yukawa potential underestimates the harmonic emission rates by many orders of magnitude, due to the lack of near-resonant rate-enhancing excited states. The relative spectra, however, are comparable and, in particular, the numbers of the last harmonics that are clearly discernible above the background are almost identical.

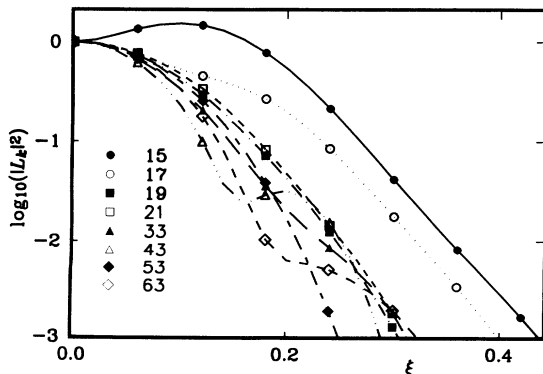


FIG. 12. Harmonic emission rate of various harmonics vs ellipticity ξ , for $|E_0|/\omega=11.1$, $\eta=42$. The figure corresponds to Fig. 2 of Ref. [74] (neon, 825 nm).

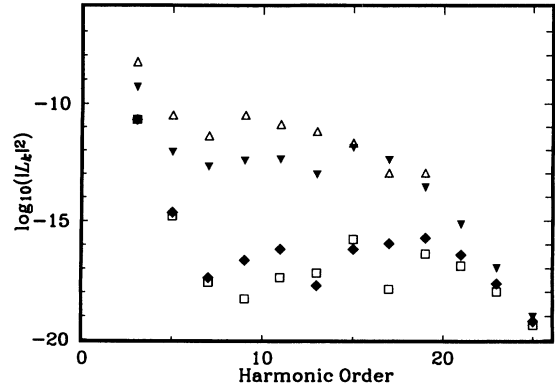


FIG. 13. The harmonic components of the dipole moment calculated using the explicit solution of the time-dependent Schrödinger equation by Kulander, Schafer, and Krause (Ref. [70]) for a Yukawa potential with one bound state (open squares) and a Coulomb potential (open triangles) both with a binding energy of 13.6 eV compared with the δ -function potential model for binding energies of 13.6 eV (filled diamonds) and $10.2 \text{ eV} = \frac{3}{4} \times 13.6 \text{ eV}$ (filled triangles); the latter number corresponds to the energy difference from the ground state to the first excited state of hydrogen. The data points of Kulander, Schafer, and Krause, which were listed with arbitrary units, have been scaled so that the third harmonic of the Yukawa potential and the 13.6-eV δ -function potential match.

There is no compulsory reason as to why in adjusting this model to a given atom we have to identify $|E_0|$ with the binding energy of the atomic ground state. Indeed, we argue in Appendix C that for the purpose of describing high-order harmonic generation, $|E_0|$ should rather be adjusted to the energy difference between the ground state and the first excited state. Figure 13 shows that this yields spectra which agree with those calculated numerically for hydrogen [70] within less than two orders of magnitude. For a Yukawa potential with just one bound state and the δ -function potential adjusted to the *same* bound-state energy the discrepancies are within the same range.

Macklin, Kmetec, and Gordon [21] have carried out a very detailed comparison between their measurements at 800 nm in neon with the predictions of this model which was used to provide the single-atom dipole input for the propagation model of Ref. [26]. The measurements of Macklin, Kmetec, and Gordon represent, at the time of this writing, the most extensive investigation of the intensity dependence of very high harmonics. They followed the 31st, 41st, ..., 101st harmonic from their respective appearance intensity up to the intensity region where the harmonic response becomes flat, that is, well inside the plateau. For the comparison with the δ -function model adjusted to the binding energy of neon, they integrated the fixed-intensity dipole response [as given in Eq. (3.15)] over the intensity distribution in the interaction region. They made the assumption that their measured intensities were too high by 40% for the 31st to 51st harmonic and by 40% for the 61st to 81st harmonic and multiplied the calculated response by relative factors of 1, 1.1, 1.9,

10.5, 14, and 7 for the 31st to 81st harmonic, respectively. The last-mentioned numbers may partly reflect the unknown relative wavelength sensitivity of their detection system. Under these conditions they obtained a very good fit of the intensity dependence of the observed harmonic response ranging from the initial rise of the harmonics with a power of the intensity near the one predicted by perturbation theory to the much flatter increase when the respective harmonics reached the plateau. Saturation was neglected in this calculation.

These comparisons suggest that the atomic binding potential strongly affects the absolute magnitude of the harmonic response, particularly the height of the plateau, and to a much lesser degree the relative harmonic spectra. As argued in Appendix C, near-resonant energy denominators have a dominant effect on the magnitude of the harmonic response. Therefore, the agreement between the data for a particular atom (or computer simulations of the same situation) and the results of the δ -function potential is significantly improved if the parameter $|E_0|$ is adjusted to the energy difference between the ground state and the first excited state rather than to the binding energy.

Finally, we can compare the results of this model to recent measurements where the effects of the ellipticity of the incident laser field on the harmonic spectrum have been investigated [74]. Figures 11 and 12 give the results of the zero-range potential for the cases of Figs. 1 and 2 of Ref. [74]. For comparison with the data, we have in each case adjusted the binding energy $|E_0|$ to the energy difference from the ground state to the first excited state of the respective atom, as discussed above.

An expansion of Eq. (3.15) (with $a_n=0$ for $n \neq 0$) to lowest order in η shows that

$$|\mathbf{d}_k|^2 \sim \xi^{2k}, \quad (4.6)$$

in agreement with an earlier estimate [75]. It can also be seen from Eq. (3.15) that there is symmetry with respect to $\xi \rightarrow -\xi$. We will therefore plot results only for positive values of ξ .

Figure 11, which is for $\epsilon=4$ and $\eta=1$, plots the total harmonic intensity, viz., the sum of the x and the y components, versus the ellipticity ξ for the 9th, 11th, and 13th harmonics, which lie beyond the plateau. At $\xi=0.5$, the calculated relative harmonic intensities exceed the lowest-order perturbation-theory (LOPT) estimate (4.6) by less than 20%. The corresponding measured relative intensities (Fig. 1 of Ref. [74]), on the other hand, exceed LOPT by a factor of 3. Figure 12 is for a substantially higher intensity ($\epsilon=11.1$ and $\eta=42$) and corresponds to Fig. 2 of Ref. [74]. All of the depicted harmonics now lie within the plateau. Our results reproduce the experimental observation that the measured harmonics split in two groups: the lower ones (the 15th and 17th) and the others. As in the case of Fig. 12, the intensities calculated from the zero-range potential fall off faster with increasing ellipticity than is shown by the data [74]. This is what one would expect to happen, from the point of view of a classical model, for a zero-range potential (see the discussion at the end of Sec. V). Figure 12

displays a lot of structure for which we have no physical explanation, such as the initial *increase* of the intensity of the 15th harmonic with increasing ellipticity and the pronounced shoulders visible for the 33rd to 63rd harmonics.

V. APPROXIMATION FOR THE HIGH HARMONICS AND A CLASSICAL MODEL

One of the characteristics of higher-harmonic emission of laser-irradiated atoms is the existence of the three distinctly different regions of the harmonic spectrum: the low harmonics where the intensity rapidly decreases with increasing harmonic number, the plateau region, and the region beyond the plateau where again the intensity quickly drops for each higher harmonic. In this section we will consider the last mentioned region. A glance at the explicit results displayed in Sec. IV shows that in this region the dependence of the harmonic spectrum on the harmonic number and the other parameters is quite smooth. Hence, it is not too surprising that for this region we will be able to find an excellent analytic approximation to the dipole moment. Fortunately, it will turn out that this approximation still holds in the uppermost part of the plateau, thus covering what might be the most interesting part of the harmonic spectrum.

We will restrict ourselves to the case where the approximation $a_n = a_0 \delta_{n0}$ holds. The integral (3.15) is largely dominated by the behavior of the Bessel functions $J_{k+1}(z(\tau))$ and $J_k(z(\tau))$ with the argument

$$z(\tau) = \eta \xi \left[\sin \tau - \frac{4 \sin^2(\tau/2)}{\tau} \right]. \quad (5.1)$$

The absolute value of $z(\tau)$ has maxima for $\tau \equiv \tau_n$ which are independent of k , η , and E_0 . These values are solutions of

$$\frac{dz}{d\tau} = -\eta \xi \left[\cos \tau_n + \frac{4}{\tau_n^2} \sin^2 \tau_n / 2 - \frac{4}{\tau_n} \sin(\tau_n/2) \cos(\tau_n/2) \right] = 0. \quad (5.2)$$

This condition can be rewritten as

$$\frac{2}{\tau_n} \sin(\tau_n/2) - \cos(\tau_n/2) = \pm \sin(\tau_n/2). \quad (5.3)$$

The corresponding values of $z(\tau_n)$ and its second derivative are

$$z(\tau_n) = 2\eta \xi \sin(\tau_n/2) \left[\cos(\tau_n/2) - \frac{2 \sin(\tau_n/2)}{\tau_n} \right] = \mp 2\eta \xi (\sin(\tau_n/2))^2, \quad (5.4)$$

$$\ddot{z}(\tau_n) = -\eta \xi \sin \tau_n. \quad (5.5)$$

There are two sets of solutions to Eq. (5.3), corresponding to the two signs in Eq. (5.3), which we will denote by $\tau_{n,\pm}$ ($n=1, 2, \dots$). It is easy to see that

$$\tau_{1,+} < \tau_{1,-} < \tau_{2,+} < \tau_{2,-} < \dots \quad (5.6)$$

For large τ , $z(\tau)$ approaches $\eta\zeta \sin\tau$ and hence $\tau_{n,+} \rightarrow (2n - \frac{1}{2})\pi$ and $\tau_{n,-} \rightarrow (2n + \frac{1}{2})\pi$. The lowest solutions $\tau_{n,\pm}$ are given in Table I, along with the corresponding values $z_{n,\pm} \equiv z(\tau_{n,\pm})$. We notice that in general $|z_{n,+}| > |z_{n,-}|$. The solution with the largest associated value $z(\tau_n)$ is

$$\tau_{1,+} = 4.0856 \quad \text{with } z_{1,+} = -1.5866\eta\zeta. \quad (5.7)$$

This $|z_{1,+}|$ constitutes an upper bound of $|z(\tau)|$ for all τ .

For later use, we still compute

$$\begin{aligned} & \frac{d}{d\tau} \left[\tau - \frac{4 \sin^2(\tau/2)}{\tau} \right] \Bigg|_{\tau=\tau_n} \\ &= \left[1 + \frac{1}{\eta\zeta} \frac{dz}{d\tau} - \frac{d \sin\tau}{d\tau} \right] \Bigg|_{\tau=\tau_n} \\ &= 1 - \cos\tau_n = 2 \sin^2\tau_n / 2 \\ &= \mp \frac{z(\tau_n)}{\eta\zeta}, \end{aligned} \quad (5.8)$$

where in the last step Eq. (5.4) has been used. In Eq. (5.8) the upper (lower) sign holds for $\tau = \tau_{n,+}$ ($\tau = \tau_{n,-}$).

For $|z| \ll k$, the Bessel function $J_k(z)$ steeply increases with increasing argument as exhibited, e.g., by the lowest term of its power-series expansion, that is,

$$J_k(z) \sim \frac{1}{k!} \left[\frac{z}{2} \right]^2 \left[1 + O\left[\frac{z^2}{k} \right] \right]. \quad (5.9)$$

Since $|z(\tau)|$ has the just mentioned upper bound of $1.5866 \eta\zeta$, we are certainly in this regime as soon as $k \gg 1.59\eta\zeta$. The integral (3.15) will then receive its dominant contributions from the maxima of $J_k(z(\tau))$ which, in turn, occur for the maxima of $|z(\tau)|$. This means that the $J_k(z)$ can be approximated by a series of peaks at $\tau = \tau_{n,\pm}$, cf. Fig. 14. The figure also shows that the peaks at $\tau = \tau_{n,+}$ dominate the peaks at $\tau = \tau_{n,-}$ since, in view of Table I, $|z_{n,+}| > |z_{n,-}|$. In this case, for moderate intensities, the peak at $\tau_{1,+}$ is by far the strongest. We will approximate $J_k(z(\tau))$ by a series of Gaussians centered at

$$\tau = \tau_{n,\pm} \equiv \bar{\tau}, \quad (5.10)$$

with appropriate widths $b \equiv b_k(\bar{\tau})$ determined by match-

$$\begin{aligned} A_k \cong & (-i)^k \frac{e^{-i\pi/4}}{2\bar{\tau}^{3/2}} \sum_{\bar{\tau}} J_k(\bar{z}) \left[\frac{\pi}{bk} \right]^{1/2} \left[\left[\frac{1}{1-\omega/\Omega} - \frac{i}{\bar{\tau}} \right] e^{i(\Omega/2\omega-1/2)\bar{\tau}} (e^{i\bar{\epsilon}} e^{-\delta_-^2/4bk} + i(-1)^k e^{-i\bar{\epsilon}} e^{-\gamma_-^2/4bk}) \right. \\ & \left. + \frac{i}{\bar{\tau}} e^{i[(\Omega/2\omega)+1/2]\bar{\tau}} (e^{i\bar{\epsilon}} e^{-\delta_+^2/4bk} + i(-1)^k e^{-i\bar{\epsilon}} e^{-\gamma_+^2/4bk}) \right], \end{aligned} \quad (5.15)$$

with

$$\gamma_{\pm} = \frac{|E_0|}{\omega} + \frac{|\bar{z}|}{\zeta} - \frac{\Omega}{2\omega} \mp \frac{1}{2}, \quad (5.16)$$

$$\delta_{\pm} = \frac{|E_0|}{\omega} + \frac{|\bar{z}|}{\zeta} + \frac{\Omega}{2\omega} \pm \frac{1}{2}, \quad (5.17)$$

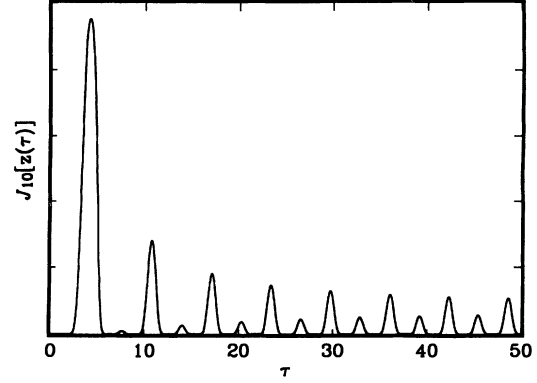


FIG. 14. $J_{10}(z(\tau))$ as a function of τ for $\eta=6$. The integral (3.15) for the harmonic emission rates receives its dominant contributions from the maxima at times $\tau = \tau_{n,\pm}$. These are the times when, in a classical picture, the electron returns to the site of the potential.

ing the second derivatives. The approximation then is

$$J_k(z(\tau)) \sim \sum_{\bar{\tau}} J_k(\bar{z}) \exp(-bk(\tau - \bar{\tau})^2), \quad (5.11)$$

with $\bar{z} \equiv z(\bar{\tau})$ and

$$b = -\frac{1}{2k} \ddot{z}(\bar{\tau}) \frac{J_k'(\bar{z})}{J_k(\bar{z})} = \frac{1}{2k} \eta\zeta \sin(\bar{\tau}) \frac{J_k'(\bar{z})}{J_k(\bar{z})}, \quad (5.12)$$

where Eq. (5.5) has been used. For $\bar{z} \ll k$, b is independent of k . In the integral in Eq. (3.16), $J_k(z(\tau))$ is multiplied by exponentials and powers. We replace powers τ^α by $\bar{\tau}^\alpha$ and exponentials according to

$$e^{if(\tau)} \cong e^{if(\bar{\tau})} e^{if'(\tau)(\tau - \bar{\tau})}, \quad (5.13)$$

and extend the integration to $-\infty$. Moreover, we drop the term with the Bessel function $J_{k+1}(z(\tau))$ as, in view of the approximation (5.9), it is smaller than $J_k(z(\tau))$ by a factor of $z/(2(k+1))$. With these approximations the relevant integral

$$A_k = \int_0^\infty \frac{d\tau}{\tau^{3/2}} e^{i(\Omega/2\omega)\tau} J_k(z(\tau)) \beta_-(\tau) \cos\alpha_{k00}(\tau) \quad (5.14)$$

is approximated by

and

$$\bar{\epsilon} = \frac{|E_0|}{\omega} \bar{\tau} + \eta\bar{\tau} \left[1 - \left[\frac{\sin(\bar{\tau}/2)}{\bar{\tau}/2} \right]^2 \right]. \quad (5.18)$$

In obtaining Eqs. (5.16) and (5.17) we make use of Eq. (5.8). For

$$\frac{|E_0|}{\omega} + \frac{|\bar{z}|}{\xi} \gg 1 \quad (5.19)$$

and $\Omega \gg 2\omega$ we have $|\gamma_{\pm}| \ll |\delta_{\pm}|$. We may then drop in Eq. (5.15) the terms involving $\exp(-\delta_{\pm}^2/4bk)$. In order to obtain an approximation valid for the end of the plateau we may also restrict the sum over $\bar{\tau}$ in Eq. (5.15) to just $\bar{\tau} = \tau_{1,+}$. Then

$$\bar{z} = -1.5866\eta\xi, \quad (5.20)$$

$$\bar{\epsilon} = \frac{|E_0|}{\omega} \bar{\tau} + 3.309\eta, \quad (5.21)$$

$$\gamma_{\pm} = \frac{|E_0|}{\omega} - \frac{\Omega}{2\omega} \mp \frac{1}{2} + 1.5866\eta, \quad (5.22)$$

and the approximation reads [recall $\Omega = (2k+1)\omega$]

$$A_k \cong i^{k+1} \frac{e^{-i\pi/4}}{2\bar{\tau}^{3/2}} J_k(\bar{z}) \left[\frac{\tau}{bk} \right]^{1/2} e^{ik\bar{\tau}} e^{-i\bar{\epsilon}} \times \left[\left[1 + \frac{1}{2k} - \frac{i}{\bar{\tau}} \right] e^{-\gamma_-^2/4bk} + \frac{i}{\bar{\tau}} e^{i\bar{\tau}} e^{-\gamma_+^2/4bk} \right]. \quad (5.23)$$

A very crude estimate of the maximum of $|A_k|$ with respect to k can be obtained as follows. The magnitude of $|A_k|$ is predominantly determined by the product $J_k(\bar{z}) \exp(-\gamma_-^2/4bk)$. The Bessel function assumes its maximum for $k \sim |\bar{z}|$ while the exponential does so for $k = |E_0|/\omega + |\bar{z}|/\xi \geq |\bar{z}|$. The maximum of the product will occur about halfway in between, i.e., at

$$k = \frac{1}{2} \frac{|E_0|}{\omega} + \frac{1}{2} (1 + \xi) \times 1.5866\eta. \quad (5.24)$$

This estimate is supported by the numerical results to be discussed below. The result (5.24) seems to imply that even in the limit where ξ goes to zero (circular polarization) harmonics are still emitted. The estimate does not take into account that for decreasing ξ the intensity of the harmonics quickly decreases so as to vanish completely in the limit of a circularly polarized field.

In Fig. 15, the approximation (5.23) is compared with an exact evaluation of Eq. (3.15). As expected, the approximation works best beyond the plateau, but is already quite good around its upper edge.

The emission of the highest harmonics near the end of the plateau can be quite well understood in terms of a simple classical model which was advanced by Kulander and co-workers [24,25]. We restrict ourselves to linear polarization, viz., $\xi = 0$ or $\xi = 1$, in what follows. The model assumes that at some time $t = t_0$ the electron is set free in the continuum with velocity zero. From this time on we neglect the atomic binding potential and consider

$$\frac{\partial}{\partial(\omega t_0)} E_{\text{kin}}(t_1) = \frac{\partial}{\partial(\omega t_0)} 2U_p(\cos\omega t_1 - \cos\omega t_0)^2$$

$$= 4U_p(\cos\omega t_1 - \cos\omega t_0) \left[-\sin\omega t_1 \left[\frac{\partial t_1}{\partial t_0} \right] + \sin\omega t_0 \right] = 0. \quad (5.29)$$

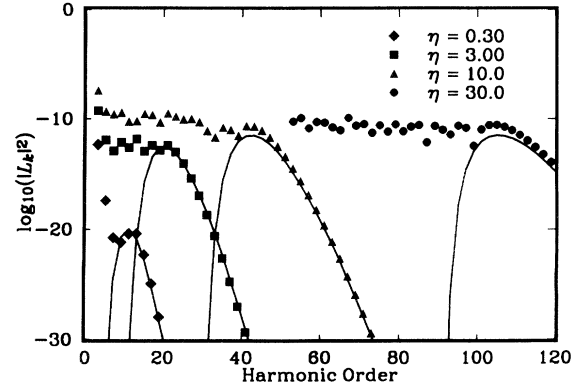


FIG. 15. Comparison of the approximation, Eq. (5.23), and the exact integral (4.1) as a function of the harmonic order $(2k+1)$ for a binding energy of $|E_0|/\hbar\omega = 10$ at selected intensities.

the electron moving classically in the presence of the laser field only, so that

$$\dot{x}(t) = -\frac{ea}{m}(\cos\omega t - \cos\omega t_0) + \dot{x}(t_0), \quad (5.25)$$

where, by assumption of the model, $\dot{x}(t_0) = 0$. We obtain a first estimate of the maximal energy that the electron can emit by calculating the time-averaged kinetic energy of the electron moving according to Eq. (5.25). This is

$$\langle E_{\text{kin}} \rangle = \frac{m}{2} \langle \dot{x}(t)^2 \rangle = \frac{(ea)^2}{2m} \left(\frac{1}{2} + \cos^2\omega t_0 \right) = U_p(1 + 2\cos^2\omega t_0). \quad (5.26)$$

Depending on the time t_0 at which the electron was set free, its time-averaged kinetic energy varies between U_p and $3U_p$. The maximal energy that the electron can emit occurs in this picture if it falls back into the atomic ground state. This energy is

$$E_{\text{max}} = |E_0| + 3U_p \cong (2k_{\text{max}} + 1)\omega. \quad (5.27)$$

A more refined version of this model [25] takes into account that the electron is most likely to emit the harmonic photon when it is within the range of the atomic binding potential, that is, for our zero-range potential when it is back at the origin. Rather than averaging the kinetic energy over time, we then determine the time t_1 of emission from the condition that for given t_0 ,

$$x(t_1) = -\frac{ea}{m\omega}(\sin\omega t_1 - \sin\omega t_0) + \frac{ea}{m}(t_1 - t_0)\cos\omega t_0 = 0. \quad (5.28)$$

This has solutions $t_1 = t_1(t_0)$. We then look for the extrema of the kinetic energy at $t = t_1$ with respect to t_0 :

Differentiating Eq. (5.28) with respect to t_0 , we determine $\partial t_1 / \partial t_0$:

$$(\cos \omega t_1 - \cos \omega t_0) \frac{\partial t_1}{\partial t_0} = -\omega(t_1 - t_0) \sin \omega t_0. \quad (5.30)$$

Equation (5.29) with (5.30) and (5.28) then provide two equations for t_0 and t_1 under the condition that $E_{\text{kin}}(t_1)$ is extremal,

$$\begin{aligned} \cos \omega t_1 - \cos \omega t_0 &= -\omega(t_1 - t_0) \sin \omega t_1, \\ \sin \omega t_1 - \sin \omega t_0 &= \omega(t_1 - t_0) \cos \omega t_0. \end{aligned} \quad (5.31)$$

In terms of the sum and difference variables

$$\tau = \omega(t_1 - t_0), \quad \sigma = \omega(t_1 + t_0), \quad (5.32)$$

Eqs. (5.31) read

$$\begin{aligned} \left[\sin \frac{\tau}{2} - \frac{\tau}{2} \cos \frac{\tau}{2} \right] \sin \frac{\sigma}{2} &= \frac{\tau}{2} \sin \frac{\tau}{2} \cos \frac{\sigma}{2}, \\ \frac{\tau}{2} \sin \frac{\tau}{2} \sin \frac{\sigma}{2} &= \left[\sin \frac{\tau}{2} - \frac{\tau}{2} \cos \frac{\tau}{2} \right] \cos \frac{\sigma}{2}, \end{aligned} \quad (5.33)$$

so that the solutions are determined by

$$\sin \frac{\tau}{2} - \frac{\tau}{2} \cos \frac{\tau}{2} = \pm \frac{\tau}{2} \sin \frac{\tau}{2}, \quad (5.34)$$

and consequently

$$\tan \frac{\sigma}{2} = \pm 1. \quad (5.35)$$

Equation (5.34) is identical with Eq. (5.3) which determines the maxima of the argument $|z(\tau)|$ of the Bessel functions in the integral (3.15). Hence the solutions are the $\tau_{n,\pm}$ tabulated in Table I. The corresponding solutions for the sum variables σ are

$$\sigma_{n,\pm} = \pm \frac{\pi}{2} + 2k\pi \quad (5.36)$$

with any integer k . The table also lists the corresponding kinetic energies

$$\begin{aligned} E_{\text{kin}}(t_1) &= 2U_p (\cos \omega t_1 - \cos \omega t_0)^2 \\ &= 8U_p \sin^2 \frac{\sigma}{2} \sin^2 \frac{\tau}{2} \\ &= 4U_p \sin^2 \frac{\tau}{2} \\ &= \mp 2\omega z(\tau_{n,\pm}) / \xi. \end{aligned} \quad (5.37)$$

In the third and last lines of the preceding equation, Eqs. (5.36) and (5.4) have been used, respectively.

We see that the quantum-mechanical integral (3.15) receives its dominant contributions from those values of τ that in the classical model correspond to a time difference between ejection of the electron into the continuum and its recurrences to the site of the nucleus, such that the kinetic-energy gain is stationary. The second derivatives of the kinetic energies are

$$\frac{\partial^2 E_{\text{kin}}(t_1)}{\partial (\omega t_0)^2} = 4U_p \frac{\tau(\tau \mp 1)}{1 \mp \tau/2} \cos^2 \frac{\tau}{2}, \quad (5.38)$$

so that the τ_+ yield maxima and the τ_- minima of the kinetic energy. According to Table I, the first recurrence time $\tau_{1,+}$ yields the highest possible kinetic energy, viz.,

$$E_{\text{kin}}(t_1) = 4U_p \sin^2 \frac{\tau_{1,+}}{2} = 3.173U_p, \quad (5.39)$$

slightly larger than the crude estimate (5.24). Hence, Eq. (5.39) specifies the upper edge of the plateau in this classical model. The model also predicts a minimal kinetic energy of $1.54U_p$. This is not related to any feature of the integral (3.15). The classical model and the approximation are just not applicable for these comparatively low harmonics.

Figure 16 depicts the contributions from some of the higher peaks. The absolute value of each is plotted separately; of course, Eq. (5.15) states that, actually, they have to be added coherently. There is some tendency of the higher peaks to fill in lower parts of the plateau down to a harmonic energy of about $|E_0|/\omega + 1.5\eta$.

Physically, from the correspondence developed thus far between the peaks of the integral (3.15) and the return times of some classical orbits, we can draw some conclusions. For the uppermost part of the plateau, the classical picture elaborated above appears to be quite close to reality. According to it, this part is due to electrons set free in the continuum at such a time that their kinetic energy, when they *first* return to the nucleus, is maximal. For the lower portions of the plateau, there is still some truth in the picture that they are emitted at *subsequent* recurrences to the nucleus. For the lower half of the plateau, below approximately $|E_0|/\omega + 1.5\eta$, this classical picture fails.

Sometimes it is assumed that this classical model applies for high intensities such that the electron appears in the continuum via tunneling ionization. Figure 15 shows that this is not necessarily the case. The approximation works very well already for intensities which clearly cor-

TABLE I. Recurrence times $\tau_{n,\pm}$ and associated values of $z(\tau)$ and the respective kinetic energies at the recurrence times.

n	$\tau_{n,+}$	$z(\tau_{n,+})/\eta\xi$	$E_{\text{kin}}(\tau_{n,+})/U_p$	$\tau_{n,-}$	$z(\tau_{n,-})/\eta\xi$	$E_{\text{kin}}(\tau_{n,-})/U_p$
1	4.086	-1.587	3.173	7.623	0.771	1.542
2	10.792	-1.202	2.404	14.004	0.867	1.735
3	17.155	-1.123	2.247	20.327	0.906	1.813
$\gg 1$	$(2n - \frac{1}{2})\pi$	-1	2	$(2n + \frac{1}{2})\pi$	+1	2

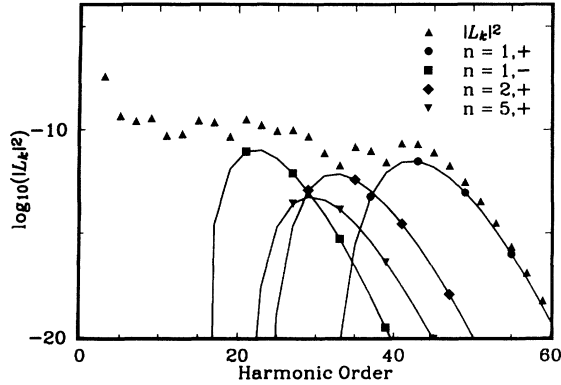


FIG. 16. Contributions from some of the higher-order maxima of $z(\tau_{n,\pm})$ to the exact integral for $\eta=10$, $|E_0|/\hbar\omega=10$.

respond to the multiphoton regime.

The classical model discussed here is very reminiscent of a similar two-step model for above-threshold ionization [71]. In this case, it was assumed that the electron was injected into the lowest possible continuum state and developed from there on according to a Volkov solution subject to the field only. For linear polarization, this model led to a fairly good description of the electron energy distribution [72]. This brings us to a limitation of these simple two-step models when it comes to their applicability to real atoms: they only work well for linear polarization [73]. For circular and already for elliptic polarization, the model assumptions are not justified. First, the electron cannot be injected any more into the continuum with zero or near zero angular momentum. Hence, the assumption of an initial zero velocity is unattainable. Second, only a few electron trajectories ever return to the site of the nucleus, not enough to yield a stationary value of the kinetic energy with respect to the injection time. This is the case for two-color high-order harmonic production to be discussed in a separate paper. It is also the case for harmonic production by an elliptically polarized laser field, which we discussed in Sec. IV. The classical model would predict virtually no harmonic production in either case. Equation (3.15) (and a similar equation for the two-color case), on the other hand, yield significant harmonic emission. However, the model might still hold if the electron is no longer required to return to the exact center of the binding potential, but only to come close. If such a picture is valid, it might explain why the zero-range potential gives significantly lower harmonic emission rates for nonzero ellipticity than recent experiments have measured [74]; it is much more difficult for the electron to return to within the range of a zero-range potential than to a Coulomb potential.

VI. CONCLUSIONS

The potential that we have used in this paper to model higher-harmonic production arguably constitutes the simplest possible description of an atom. This has two immediate advantages. First, the model yields expres-

sions for the rates of emission of higher harmonics in closed form, that is, just one quadrature is left for numerical evaluation. These integrations typically run on a workstation not much longer than a few seconds depending on the parameters. They require nothing more than a reliable integration routine, as opposed to the numerous subtleties involved in a high-precision numerical solution of the Schrödinger equation. Moreover the model is truly three dimensional. Second, the model provides a good deal of physical insight in the following sense. Whichever qualitative features it yields do not depend on any more complicated properties of the atom than the very facts that (i) it binds and (ii) it can be ionized. Effects present in the data but not in this model then have to be attributed to the detailed atomic structure. For example, such a model is not capable of pinpointing the consequences of resonances with excited states which from the point of view assumed above may be considered a virtue. The model should provide a good description of harmonic production in negative ions such as H^- . Finally, it has turned out [21] that it even gives a good description of the relative intensities of high-order harmonic production in atoms over a large range of harmonics and laser intensities. Probably still better agreement with the data would result if the ground-state energy of the model would be adjusted to the energy difference between the ground state and the first excited state of the atom rather than to its binding energy, as we proposed in this paper.

ACKNOWLEDGMENTS

One of us (W.B.) is indebted to M. Kleber and the theory division of the Munich Technical University for their hospitality and for stimulating discussions. W.B. also acknowledges partial support from the Sonderforschungsbereich SFB 338 of the Deutsch Forschungsgemeinschaft.

APPENDIX A: APPROXIMATION OF THE QUASIENERGY GROUND STATE

All of the explicit computations in this paper and all of the results are contingent upon the approximation $a_n = a_0 \delta_{n0}$, that is, we replaced the function $R(t)$ defined in Eq. (2.14) by $a_0 \exp(-iEt)$. This is exact for circular polarization but not in general. In order to obtain an accurate solution we have to solve Eq. (2.30), which involves the eigenvalue of E' in a complicated nonlinear fashion, for the expansion coefficients a_n . For the leading coefficients $a_{\pm 1}$ (and, possibly, for $a_{\pm 2}$) this can be done as outlined below Eq. (2.36). In general, however, we replace E on the right-hand side of Eq. (2.31) by its field-free value $-|E_0|$ while linearizing the left-hand side of Eq. (2.30) with respect to the quantity $\Delta - i\Gamma/2$, which when cut off can be solved by standard methods to yield the a_n . These then enter Eq. (3.15), which specifies the harmonics. We will here be satisfied with just presenting and discussing the results.

Figure 17 displays selected expansion coefficients for $|E_0|/\omega=10$. Most importantly, the a_n come out to be very small compared to unity. They can be seen to follow

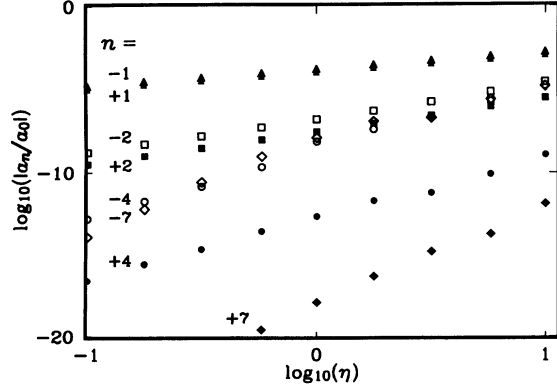


FIG. 17. The expansion coefficients $|a_n|/|a_0|$ defined in Eq. (2.26) for $|E_0|/\omega = 10$ and various values of n as a function of η .

the expected power law $a_n \sim \eta^{|n|}$ up to values of η well above unity. Moreover, for $n > 1$, we have $|a_{-n}| \gg |a_n|$. This is to be expected as the a_n with $n < 0$ correspond to virtual states above the ground-state energy $-|E_0|$. Inserting now the a_n in Eq. (3.15) we have to carry out the various integrals, all of which are of the same form as the L_k . These integrals are largest if the index of the Bessel function is zero, i.e., for $n = k$ or $k + 1$ and if

$$\int d^3r G^{(E)}(\mathbf{r}'t', \mathbf{r}t) \mathbf{r} G^{(E)}(\mathbf{r}t, \mathbf{r}''t'') = -\frac{i}{t' - t''} \left[(t - t'') \left[\mathbf{r}' + \frac{e}{m} \int_t^{t'} d\tau \mathbf{A}(\tau) \right] + (t' - t) \left[\mathbf{r}'' + \frac{e}{m} \int_t^{t''} d\tau \mathbf{A}(\tau) \right] \right] G^{(E)}(\mathbf{r}'t', \mathbf{r}''t''). \quad (\text{B2})$$

Since

$$[G^{(E)}(\mathbf{r}t, \mathbf{r}'t')]^* = -G^{(E)}(\mathbf{r}'t', \mathbf{r}t), \quad (\text{B3})$$

for the homogeneous propagator, we obtain from Eq. (B2) letting $\mathbf{r}' = \mathbf{r}'' = \mathbf{0}$ the relation

$$\int d^3r [G^{(E)}(\mathbf{r}t, 0t')]^* \mathbf{r} G^{(E)}(\mathbf{r}t, 0t'') = -\frac{ie}{m(t' - t'')} \left[(t - t'') \int_t^{t'} d\tau \mathbf{A}(\tau) + (t' - t) \int_t^{t''} d\tau \mathbf{A}(\tau) \right] G^{(E)}(0t', 0t''). \quad (\text{B4})$$

We notice that

$$\int d^3r [G^{(E)}(\mathbf{r}t, 0t')]^* e \mathbf{r} G^{(E)}(\mathbf{r}t, 0t'') = \mathbf{d}(t; t', t'') = [\mathbf{d}(t; t'', t')]^*, \quad (\text{B5})$$

where $\mathbf{d}(t; t', t'')$ has been introduced in Eq. (3.6).

APPENDIX C: PLATEAU AND LOWEST-ORDER PERTURBATION THEORY

Superficially, it appears that HHG is the paradigm of a phenomenon that cannot be explained by lowest-order perturbation theory (LOPT). On closer inspection, however, it becomes clear that some of the surprising features of HHG, in particular the fact that the harmonic production rates do not uniformly decrease with increasing order, are already ingrained in LOPT. In this appendix, we will present and discuss LOPT for the harmonics in order

$|E_0|/\omega + n + 2l \approx 0$ in Eq. (3.17), i.e., where $l \approx -\frac{1}{2}(|E_0|/\omega + k)$, $n + l \approx -\frac{1}{2}(|E_0|/\omega - k)$. The explicit evaluation shows that the error introduced by the approximation of the ground state is of relative order 10^{-2} or smaller for all harmonics but the third. In the latter case, it may be of order unity or even larger, but in any case within one order of magnitude. For example, for $\eta \lesssim 10$, the approximation underestimates the rate of emission of the third harmonic by a factor of 1.6, while for the fifth harmonic the approximation agrees with the exact result up to terms which are of relative order 10^{-2} .

APPENDIX B: A FORMAL RELATION

In this appendix, $G^{(E)}(\mathbf{r}t, \mathbf{r}'t')$ will designate the homogeneous propagator, defined again by Eqs. (2.8)–(2.12) but without the δ function on the rhs of Eq. (2.8) and without the θ function on the rhs of Eq. (2.10). This propagator satisfies

$$\int d^3r G^{(E)}(\mathbf{r}'t', \mathbf{r}t) G^{(E)}(\mathbf{r}t, \mathbf{r}''t'') = -iG^{(E)}(\mathbf{r}'t', \mathbf{r}''t''), \quad (\text{B1})$$

by virtue of being the propagator. Differentiating this equation with respect to \mathbf{r}' and \mathbf{r}'' and adding or subtracting the two resulting equations yield with the help of the explicit form (2.9)–(2.12),

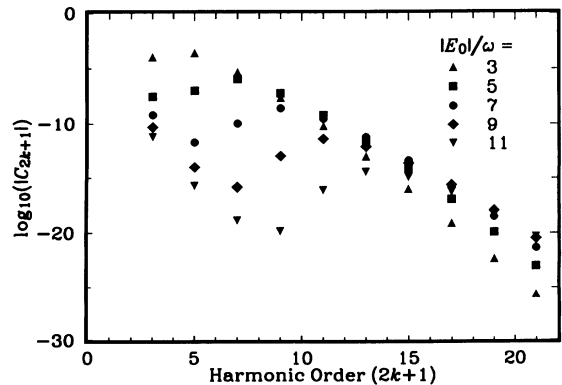


FIG. 18. Lowest-order-perturbation-theory cross sections as a function of harmonic order for selected binding energies. The cross sections rise when the harmonic order approaches the binding energy.

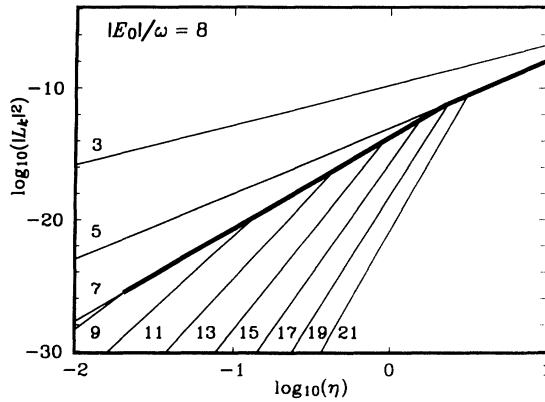


FIG. 19. $|L_k|^2$ calculated by lowest-order perturbation theory as a function of intensity for a binding energy of $|E_0|/\hbar\omega=8$. The figure displays the intensities $\eta_{7,9}$, $\eta_{7,11}$, $\eta_{7,13}$, \dots , and $\eta_{5,7}$ where LOPT rates intersect, as discussed in the text.

to elucidate the general behavior of HHG.

Figure 18 depicts the LOPT harmonic cross sections C_n , defined by

$$|L_k|^2 = C_{2k+1} \eta^{2k+1}. \quad (\text{C1})$$

This definition is somewhat arbitrary. We could have just as well included in the definition the constants displayed in Eq. (4.3), in particular the factor of $(2k+1)^3$. The data points were calculated by using a very low intensity, viz. $\eta=0.01$. They agree with what would have resulted from true LOPT. Figure 18 exhibits a dramatic rise of the harmonic cross sections whenever the harmonic order approaches and exceeds $|E_0|/\omega$. Similar results have been encountered in early calculations based on LOPT [39–41]. The physical reason is obvious if one envisions the analytic expression for the LOPT cross section: as soon as $n \geq |E_0|/\omega$, real intermediate states contribute. Figure 19 provides for another view of the same situation from a different angle. Here the quantities $|L_k|^2$ as obtained from LOPT are plotted versus η . On the doubly logarithmic scale of the figure they are represented by straight lines with a slope of $2k+1$. However, owing to the dependence of the cross sections C_{2k+1} on k , all of the straight lines with $n=2k+1 < |E_0|/\omega$ intersect those with $n > |E_0|/\omega$. The intersection that occurs for the lowest value of η is between those harmonics whose order is just above and just below $|E_0|/\omega$. In the case depicted where $|E_0|/\omega=8$, these are $n=7$ and $n=9$ and we refer to the corresponding intensity parameter by $\eta_{7,9}$. For laser intensities higher than this point of intersection, according to LOPT, the intensity of the ninth harmonic would exceed that of the seventh. This defines the likely

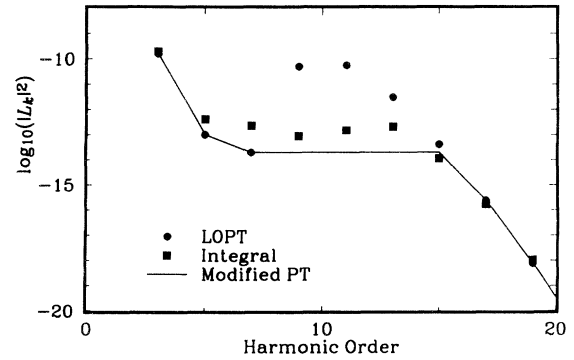


FIG. 20. Comparison of $|L_k|^2$ obtained from lowest-order perturbation theory (dots), the exact integral (squares), and “modified” perturbation theory where the plateau is set to the level of its lowest member (line).

point of departure from LOPT for the ninth harmonic, *not for the seventh*, which keeps following LOPT until at a much higher laser intensity $\eta_{5,7}$, it intersects the fifth harmonic. It is at the intensity corresponding to $\eta_{7,9}$ that the plateau begins to form. As the intensity increases, the higher harmonics one at a time intersect the seventh, at intensities $\eta_{7,11}, \eta_{7,13}, \dots$. The procedure is more easily read off from the figure than explained in words. Figure 20 demonstrates that it is not a bad approximation to describe the entire plateau by LOPT for its lowest member. If we plot, for fixed η , the harmonic intensities versus the harmonic number it boils down to approximating the plateau by a horizontal line extending to the right starting from the lowest harmonic beyond which the LOPT harmonic intensities start rising.

The conclusions to be drawn from these observations are somewhat counterintuitive; the harmonics outside the plateau, both the lower and the higher ones, follow LOPT. (The fact that the high harmonics beyond the plateau do so has already been clear from the approximation discussed in Sec. V; cf. Eq. (5.23) and notice that beyond the plateau the Bessel function can be replaced by the leading term of its power-series expansion.) The harmonics within the plateau region are *deemphasized* by the departure from LOPT (rather than enhanced, as one might expect at first glance); LOPT predicts a mountain where the exact calculation yields the plateau. For low laser intensities, the plateau starts to form at $n \approx |E_0|/\omega$. With increasing intensity it grows both towards lower- and towards higher-harmonic numbers, though much faster towards the higher harmonics. With respect to the laser intensity η , the plateau roughly scales with the harmonic number n_{\min} of its lowest member, that is, with $\eta^{n_{\min}}$.

[1] *Atoms in Intense Fields*, edited by M. Gavrila, *Advances in Atomic, Molecular, and Optical Physics, Supplement* (Academic, London, 1992).

[2] N. B. Delone and M. V. Fedorov, *Usp. Fiz. Nauk* **158**, 215

(1989) [*Sov. Phys. Usp.* **32**, 500 (1990)].

[3] J. Javanainen, J. H. Eberly, and K. Rzażewski, *Phys. Rep.* **204**, 331 (1991).

[4] G. Mainfray and C. Manus, *Rep. Prog. Phys.* **54**, 1333

- (1991).
- [5] R. R. Freeman and P. H. Bucksbaum, *J. Phys. B* **24**, 325 (1991).
- [6] A. L'Huillier, K. J. Schafer, and K. C. Kulander, *J. Phys. B* **24**, 3315 (1991).
- [7] A. L'Huillier, L.-A. Lompré, G. Mainfray, and C. Manus, in *Advances in Atomic, Molecular, and Optical Physics, Supplement* (Ref. [1]), p. 139.
- [8] H. R. Reiss, *Prog. Quantum Electron.* **16**, 1 (1992).
- [9] K. Burnett, V. C. Reed, and P. L. Knight, *J. Phys. B* **26**, 561 (1993).
- [10] M. G. Groseva, D. I. Metchkov, V. M. Mitev, L. I. Pavlov, and K. V. Stamenov, *Opt. Commun.* **23**, 77 (1977).
- [11] J. Reintjes, C. She, and R. Reckardt, *IEEE J. Quantum Electron.* **QE-14**, 581 (1978).
- [12] J. Bokor, P. H. Bucksbaum, and R. R. Freeman, *Opt. Lett.* **8**, 217 (1983).
- [13] J. Wildenauer, *J. Appl. Phys.* **62**, 41 (1987).
- [14] A. McPherson, G. Gibson, H. Jara, U. Johann, T. S. Luk, I. A. McIntyre, K. Boyer, and C. K. Rhodes, *J. Opt. Soc. Am. B* **4**, 595 (1987).
- [15] M. Ferray, A. L'Huillier, X. F. Li, L.-A. Lompré, G. Mainfray, and C. Manus, *J. Phys. B* **21**, L31 (1988).
- [16] X. F. Li, A. L'Huillier, M. Ferray, L.-A. Lompré, and G. Mainfray, *Phys. Rev. A* **39**, 5751 (1989).
- [17] L.-A. Lompré, A. L'Huillier, M. Ferray, P. Monot, G. Mainfray, and C. Manus, *J. Opt. Soc. Am. B* **7**, 754 (1990).
- [18] N. Sarakura, K. Hata, T. Adachi, R. Nodomi, M. Watanabe, and S. Watanabe, *Phys. Rev. A* **43**, 1669 (1991).
- [19] K. Miyazaki and H. Sakai, *J. Phys. B* **25**, L83 (1992).
- [20] J. K. Crane, M. D. Perry, S. Herman, and R. W. Falcone, *Opt. Lett.* **17**, 1256 (1992).
- [21] J. J. Macklin, J. D. Kmetec, and C. L. Gordon III, *Phys. Rev. Lett.* **70**, 766 (1993).
- [22] A. L'Huillier and Ph. Balcou, *Phys. Rev. Lett.* **70**, 774 (1993).
- [23] K. Kondo, N. Sarakura, K. Sajiki, and S. Watanabe, *Phys. Rev. A* **47**, R2480 (1993).
- [24] J. L. Krause, K. J. Schafer, and K. C. Kulander, *Phys. Rev. Lett.* **68**, 3535 (1992).
- [25] K. C. Kulander (unpublished).
- [26] A. L'Huillier, K. J. Schafer, and K. C. Kulander, *Phys. Rev. Lett.* **66**, 2200 (1991).
- [27] A. L'Huillier, Ph. Balcou, S. Candel, K. J. Schafer, and K. C. Kulander, *Phys. Rev. A* **46**, 2778 (1992).
- [28] K. J. Schafer, J. L. Krause, and K. C. Kulander, *Int. J. Nonlinear Opt. Phys.* **1**, 245 (1992).
- [29] L. C. Biedenharn, G. A. Rinker, and J. C. Solem, *J. Opt. Soc. Am. B* **6**, 221 (1989).
- [30] B. Sundaram and P. W. Milonni, *Phys. Rev. A* **41**, 6571 (1990).
- [31] L. Plaja and L. Roso-Franco, *J. Opt. Soc. Am. B* **9**, 2210 (1992); A. E. Kaplan and P. L. Shkolnikov, *Phys. Rev. A* **49**, 1275 (1994).
- [32] M. Yu. Ivanov and P. B. Corkum, *Phys. Rev. A* **48**, 580 (1993).
- [33] J. Z. Kamiński, *Phys. Lett. A* **151**, 308 (1990).
- [34] Q. Su and J. H. Eberly, *Phys. Rev. A* **44**, 5997 (1991).
- [35] J. H. Eberly, Q. Su, and J. Javanainen, *Phys. Rev. Lett.* **62**, 881 (1989).
- [36] J. H. Eberly, Q. Su, and J. Javanainen, *J. Opt. Soc. Am. B* **7**, 1289 (1989).
- [37] J. H. Eberly, Q. Su, J. Javanainen, K. C. Kulander, B. W. Shore, and L. Roso-Franco, *J. Mod. Opt.* **36**, 829 (1989).
- [38] R. A. Sacks and A. Szöke, *J. Opt. Soc. Am. B* **8**, 1987 (1991).
- [39] R. M. Potvliege and R. Shakeshaft, *Z. Phys. D* **11**, 93 (1989).
- [40] B. Gao and A. F. Starace, *Phys. Rev. A* **39**, 4550 (1989).
- [41] L. Pan, K. T. Taylor, and C. W. Clark, *Phys. Rev. A* **39**, 4894 (1989).
- [42] R. M. Potvliege and R. Shakeshaft, *Phys. Rev. A* **40**, 3061 (1989).
- [43] P. L. deVries, *J. Opt. Soc. Am. B* **7**, 517 (1990).
- [44] K. LaGattuta, *Phys. Rev. A* **41**, 5110 (1990).
- [45] H. Xu, X. Tang, and P. Lambropoulos, *Phys. Rev. A* **46**, R2225 (1992).
- [46] K. C. Kulander and B. W. Shore, *Phys. Rev. Lett.* **62**, 524 (1989).
- [47] J. L. Krause, K. J. Schafer, and K. C. Kulander, *Phys. Rev. A* **45**, 4998 (1992).
- [48] K. C. Kulander, K. J. Schafer, and J. L. Krause, in *Advances in Atomic, Molecular, and Optical Physics, Supplement* (Ref. [1]), p. 247.
- [49] K. Burnett, V. C. Reed, J. Cooper, and P. L. Knight, *Phys. Rev. A* **45**, 3347 (1992).
- [50] G. Bandarage, A. Maquet, and J. Cooper, *Phys. Rev. A* **41**, 1744 (1990).
- [51] G. Bandarage, A. Maquet, Th. Ménils, R. Taïeb, V. Vénier, and J. Cooper, *Phys. Rev. A* **46**, 380 (1992).
- [52] G. D. Billing, N. E. Henriksen, and C. Leforestier, *Phys. Rev. A* **45**, R4229 (1992).
- [53] F. Brunel, *J. Opt. Soc. Am. B* **7**, 521 (1990).
- [54] P. B. Corkum, N. H. Burnett, and F. Brunel, in *Advances in Atomic, Molecular, and Optical Physics, Supplement* (Ref. [1]), p. 108.
- [55] F. Giammanco, *Phys. Rev. A* **43**, 6939 (1991).
- [56] E. Fermi, *Ric. Sci.* **7**, 13 (1936).
- [57] K. Wódkiewicz, *Phys. Rev.* **43**, 68 (1991).
- [58] N. L. Manakov and L. P. Rapoport, *Zh. Eksp. Teor. Fiz.* **69**, 842 (1975) [*Sov. Phys. JETP* **42**, 430 (1976)].
- [59] I. J. Berson, *J. Phys. B* **8**, 3078 (1975).
- [60] N. L. Manakov and A. G. Fainshtein, *Zh. Eksp. Teor. Fiz.* **79**, 751 (1980) [*Sov. Phys. JETP* **52**, 382 (1981)].
- [61] W. Becker, S. Long, and J. K. McIver, *Phys. Rev. A* **42**, 4416 (1990).
- [62] W. Becker, S. Long, and J. K. McIver, *Phys. Rev. A* **41**, 4112 (1990).
- [63] W. Becker, S. Long, and J. K. McIver, *Phys. Rev. A* **46**, R5334 (1992).
- [64] W. Becker, J. K. McIver, and K. Wódkiewicz, *Laser Phys.* **3**, 475 (1993).
- [65] F. Ehlötzky, *Can. J. Phys.* **70**, 72 (1992).
- [66] K. Rzażewski and J. H. Eberly, *J. Mod. Optics* **39**, 795 (1992).
- [67] Ph. Balcou and A. L'Huillier, *Phys. Rev. A* **47**, 1447 (1993).
- [68] M. H. Mittleman, *Phys. Rev. A* **42**, 5645 (1990).
- [69] H. G. Muller and M. Gavril, *Phys. Rev. Lett.* **71**, 1693 (1993).
- [70] K. C. Kulander, K. J. Schafer, and J. L. Krause (unpublished).
- [71] W. Becker, R. R. Schlicher, and M. O. Scully, *J. Phys. B* **19**, L785 (1986).
- [72] G. Petite, P. Agostini, and H. G. Muller, *J. Phys. B* **21**, 4097 (1988).
- [73] H. G. Muller, P. Agostini, and G. Petite, in *Advances in Atomic, Molecular, and Optical Physics, Supplement* (Ref.

- [1]), p. 1.
- [74] K. S. Budil, P. Salières, A. L'Huillier, T. Ditmire, and M. D. Perry, *Phys. Rev. A* **48**, R3437 (1993).
- [75] N. L. Manakov and V. D. Ovsyannikov, *Zh. Eksp. Teor. Fiz.* **79**, 1769 (1980) [*Sov. Phys. JETP* **52**, 895 (1980)].
- [76] A. L'Huillier, M. Lewenstein, P. Salières, Ph. Balcou, M. Yu. Ivanov, J. Larsson, and C. G. Wahlström, *Phys. Rev.* **48**, R3433 (1993). These authors solve for the dipole moment in a model based on assumptions that are satisfied by the δ -function atom and our model, notably just one bound state which is not depleted. Since their model contains free propagation in the continuum just like ours, it

yields results which appear to be quite similar to ours as well. However, their explicit formula for the dipole moment [Eq. (2) of their paper] looks quite different. Comparison of the similarities and dissimilarities is easiest if we rewrite our Eq. (3.7) (assuming $a_n = \delta_{n,0} a_0$ and $E = -|E_0|$) in the form

$$x(t) = \frac{2\pi i \kappa}{\omega^2 m^3} \int_{-\infty}^t dt' dt'' \mathcal{F}(t; t', t'') \\ \times \int d^3 p \exp \left[-i \int_{t''}^{t'} d\tau \left(\frac{(\mathbf{p} - e \mathbf{A})^2}{2m} + |E_0| \right) \right].$$